HHS Public Access

Author manuscript

Nat Cell Biol. Author manuscript; available in PMC 2019 October 29.

Published in final edited form as:

Nat Cell Biol. 2019 May ; 21(5): 614–626. doi:10.1038/s41556-019-0321-6.

The lysosomal GPCR-like protein GPR137B regulates Rag and mTORC1 localization and activity

Lin Gan[1,#], **Akiko Seki**[1,#], **Kimberle Shen**[2], **Harini Iyer**[2], **Kyuho Han**[1], **Arnold Hayer**[1], **Roy Wollman**[3], **Xuecai Ge**[1], **Jerry Lin**[1], **Gautam Dey**[1], **William S. Talbot**[2], **Tobias Meyer**[1]

[1]Department of Chemical and Systems Biology, Stanford University

[2]Department of Developmental Biology, Stanford University

[3]Present address: Department of Integrative Biology and Physiology and Department of Chemistry and Biochemistry, University of California, Los Angeles

Abstract

Cell growth is controlled by a lysosomal signaling complex containing Rag small GTPases and mTORC1 kinase. Here we carried out a microscopy-based genome-wide human siRNA screen and discovered a lysosome-localized G-protein coupled receptor (GPCR)-like protein, GPR137B, that interacts with Rag GTPases, increases Rag localization and activity, and thereby regulates mTORC1 translocation and activity. High GPR137B expression can recruit and activate mTORC1 in the absence of amino acids. Furthermore, GPR137B also regulates the dissociation of activated Rag from lysosomes, suggesting that GPR137B controls a cycle of Rag activation and dissociation from lysosomes. GPR137B knockout cells exhibited defective autophagy and an expanded lysosome compartment, similar to Rag knockout cells. Like zebrafish RagA mutants, GPR137B mutant zebrafish had upregulated TFEB target gene expression and an expanded lysosome compartment in microglia. Thus, GPR137B is a GPCR-like lysosomal regulatory protein that controls dynamic Rag and mTORC1 localization and activity as well as lysosome morphology.

Keywords

mTORC1; lysosomes; Rag; nutrient sensing; mTOR signaling

INTRODUCTION

Cells regulate growth, autophagy and metabolism by employing a lysosomal regulatory complex consisting of heterodimers of Rag small GTPase proteins (one RagA/B protein

[#]These authors contributed equally to this work.

Competing Financial Interests

The authors declare no competing financial interests.

Data availability. The screen data that support the findings of this study have been deposited in the PubChem BioAssay under the accession code AID 29260. Statistical source data for Figs. 2–8 and Supplementary Figs. 1, 2, 4–6 and 8 are provided in Supplementary Table 4. All data supporting the findings of this study are available from the corresponding author upon request.

paired with one RagC/D protein)[1–3] and the cytoplasmic regulatory complex mTORC1 containing the protein kinase mTOR and an adapter protein raptor[4,5] (Fig. 1a). Rag dimers are anchored to lysosomes and activated by a lysosome-localized Ragulator adapter complex[6,7], and inactivated by a GATOR1 complex that stimulates the hydrolysis of GTP in active RagA/B-GTP to produce inactive RagA/B-GDP[8,9]. Amino acids, glucose and possibly other nutrients increase the activity of Rags and thereby recruit mTORC1 to lysosomes[4,10,11]. Active Rags also recruit and repress TFEB, a transcription factor that controls the expression of genes needed for lysosome biogenesis and function[12,13]. Once localized at lysosomes, the kinase activity of mTORC1 is regulated by growth factors through a PI3K-Akt-TSC2-Rheb signaling pathway and other mechanisms[14–17]. Nevertheless, most of the known regulators of mTORC1 are not unique to lysosomes. Only two lysosomal transmembrane proteins, the proton pump v-ATPase and the arginine transporter SLC38A9, have been shown to regulate mTORC1[18–21], suggesting that additional lysosome-specific transmembrane proteins may regulate Rag activity.

Cells with ablated Rags have expanded lysosomes, accumulated autophagosomes and increased expression of TFEB transcriptional targets but still retain some mTORC1 activity[22–25]. Knockout of two Rag regulators, WDR24 and LAMTOR1, showed similar lysosome and autophagy defects[26,27]. These studies uncovered essential functions of Rags in lysosome/autophagy regulation and point toward other mTORC1 regulators that remain to be identified.

Here we used a genome-wide siRNA screen to identify additional regulators of lysosomal mTORC1 localization and activity. We identified GPR137B, a lysosome-localized GPCR-like protein with unknown function, as a regulator that promotes recruitment and activation of mTORC1. We show that GPR137B regulates mTORC1 through Rag proteins by (1) interacting with Rag proteins and increasing Rag concentration at lysosomes and (2) increasing the GTP-loaded, active state of lysosomal RagA, which causes a recruitment of mTORC1 and an accelerated dissociation of active Rags from lysosomes. We further show that knockout of GPR137B in human cells results in a similar expansion of lysosome compartments and increased autophagy as observed in RagA/B knockout MEFs and cardiomyocytes[23]. We generated *gpr137ba* mutant zebrafish and further observed that these animals have some phenotypic similarities to *rraga* mutants, including an upregulation of TFEB target genes and an expanded lysosomal compartment phenotype in microglial cells in vivo. Together, our study introduces a GPCR-like activator of lysosomal Rag and mTORC1 signaling that regulates the dynamic exchange of active Rags at lysosomes and provides a potential therapeutic target to regulate mTORC1 activity.

RESULTS

Human siRNA screen identifies a lysosome-localized GPCR-like protein as a regulator of mTORC1

We used 21,041 pools of four siRNAs to identify mediators of amino acid signaling to mTORC1 in human fibroblasts (Hs68). Our microscopy-based assay monitored the amino acid-triggered increase in phosphorylation of the ribosomal protein S6 (rpS6) at residue 240 and 244 (Fig. 1a, b; Supplementary Fig. 1a)[28,29]. The assay captured roughly an equal

number of 1000 siRNA pools that target positive and negative regulators (Fig. 1c, Supplementary Fig. 1b and Supplementary Table 1), such as the known mTORC1 activator Rheb and suppressor TSC2 (Fig. 1c, arrows). We confirmed the screening results using individual siRNAs and narrowed our focus on 427 high confidence candidates (Supplementary Fig. 1c). Ingenuity pathway analysis showed that genes associated with insulin/growth factor, PI3K/AKT, ERK/MAPK, Hedgehog, p53, AMPK, glycine cleavage pathway and cell cycle signaling pathways were significantly enriched in the set (Supplementary Fig. 1d and Table 2).

Since amino acid-induced translocation of mTORC1 to lysosomes is a key step in the activation process[6,8], we used automated microscopy to monitor mTORC1 translocation by quantifying the co-localization between the lysosome marker Lamp2 and mTOR. To exclude indirect regulators that control amino acids uptake, we starved cells and then induced a transient increase in intracellular amino acids by inhibiting protein translation using cycloheximide[30] (Fig. 1d and Supplementary Fig. 1e). Using this assay, we screened for effects caused by the knockdown of each of the 427 candidate genes. A small subset of hits significantly reduced mTOR translocation to lysosomes as well as rpS6 phosphorylation (Fig. 1e, f), consistent with the interpretation that only some genes regulate the translocation of mTORC1 while most genes regulate mTORC1 activity after lysosome translocation (Supplementary Fig. Table 3 shows a rank-ordered list of 15 identified genes). RagC was the top hit regulating mTOR translocation in the screen, followed by less characterized candidate genes that include transporters, an anti-apoptotic factor TIAF1 and a F-box DNA helicase, suggesting that mTORC1 translocation is regulated by nutrient, metabolism and stress pathways. We focused our subsequent analysis on GPR137B, because it is lysosome-localized[31] and because it is a predicted 7-transmembrane protein with a low sequence homology to G-protein coupled receptors (GPCRs) (Fig. 2a).

GPR137B regulates lysosome localization and activity of mTORC1

Consistent with a reported lysosome localization[31], we found that GPR137B-YFP colocalized with the lysosomal marker Lamp2 and with mTOR after amino acid stimulation (Fig. 2b). We quantified the relative lysosomal localization of mTOR using a co-localization score or automated analysis of mTOR localization based on a binary lysosome mask (Supplementary Note). Independent siRNAs in two cell types (Hs68 and HeLa cells) confirmed the screening result (Fig. 2c, d and Supplementary Fig. 2a–c). Time-course analysis of rpS6 phosphorylation revealed that GPR137B knockdown reduces basal mTORC1 activity in nutrient replete cells as well as mTORC1 reactivation in nutrient-stimulated cells (Supplementary Fig. 2d). Furthermore, overexpression of GPR137B increased mTOR translocation weakly in the presence of amino acids and strongly in the absence of amino acids (Fig. 2e, f; Supplementary Fig. 2e). Finally, GPR137 and GPR137C, two genes homologous to GPR137B, likely have a similar role in regulating mTORC1 since we found that they were also lysosome-localized (Fig. 2g) and both increased mTOR translocation to lysosomes when overexpressed (Supplementary Fig. 2f, g). Together, these results suggest that GPR137B is part of a family of lysosome-localized GPCR-like proteins that regulate mTORC1 translocation to lysosomes.

An important role of mTORC1 is to inhibit autophagosome formation through phosphorylation of the ULK1-mATG13-FIP200 complex[32]. Consistent with a role of GPR137B in regulating mTORC1 activity, knocking down GPR137B increased autophagy, as indicated by an increase in the number of LC3-GFP puncta per cell (Fig. 2h). p62/SQSTM1 is an ubiquitin-binding protein that is degraded by autophagy and accumulates if autophagy flux is reduced or defective[33,10,23,25,27]. We observed a marked upregulation of p62 in GPR137B knockdown cells and the larger, brighter p62 and LC3-GFP puncta observed mostly in GPR137B depleted cells co-localize with each other (Fig. 2i, j), suggesting that autophagy flux defects contribute to the LC3 phenotype in GPR137B knockdown cells.

Translational regulators 4E-BP1 and S6K are critical mTORC1 substrate and regulator of protein synthesis and cell size[34–36]. Overexpression of GPR137B-YFP in cells starved of amino acids increased the phosphorylation of 4E-BP1 close to the level reached by amino acid stimulation (Fig. 2k and Supplementary Fig. 2h). for controlsFurthermore, biochemical analysis confirmed that knockdown of GPR137B suppresses phosphorylation of S6K and 4E-BP1 (Fig. 2l) and the GPR137B expression-mediated increase in S6K and 4E-BP1 phosphorylation was abolished upon rapamycin treatment (Fig. 2m). Finally, GPR137B mediates its effects on S6K through amino acid signaling rather than growth factor-regulation of mTORC1 (Supplementary Fig. 2i, j). Thus, GPR137B regulates amino acid-induced mTORC1 translocation to lysosomes and mTORC1 activity, and has likely a functional role in regulating autophagy as well as protein synthesis and cell size through regulation of S6K, 4E-BP1 and other mTORC1 targets.

GPR137B regulates mTORC1 localization and activity through Rag GTPases

Several lines of evidence argue that GPR137B regulates mTORC1 localization and activity through Rags. First, we used RagA/B knockout MEFs[23] and found that stable expression of GPR137B in these cells could not restore mTORC1 translocation (Fig. 3a, b, c; Supplementary Fig. 3a). Second, when we overexpressed constitutively active RagA/C (RagA-Q66L, RagC-T75N)[4] in HeLa cells, knockdown of GPR137B did not alter the increased lysosomal mTORC1 localization (Fig. 3d). In an independent strategy to activate endogenous Rags, we overexpressed GPR137B in HEK293E cells deficient for the GATOR1 component Nprl3[8,38] that have constitutively active RagA. While the wildtype cells showed a GPR137B expression-mediated increase in mTORC1 translocation, GPR137B did not cause additional mTORC1 translocation in the knockout cells (Fig. 3e). Together, these results suggest that GPR137B signals through Rag GTPases to regulate mTORC1 translocation and activity.

GPR137B interacts with Rags and increases the lysosomal localization of RagA

We next evaluated the binding interactions of GPR137B with known components of the mTORC1 regulatory machinery. In HEK293T cells, we found that GPR137B co-immunoprecipitated with mTOR, raptor, and RagA (Fig. 4a and Supplementary Fig. 3b). Control experiments using an unrelated lysosomal transmembrane protein Npc1 as well as tests using other mTORC1 regulators are shown in Supplementary Figure 4a, b.

Interestingly, when we co-expressed two GPR137B constructs with different tags, we observed an apparent amino acid-stimulated interaction of GPR137B with itself that is dependent on the presence of Rags (Fig. 4b), suggesting that more than one GPR137B protein is part of an amino acid-regulated lysosomal signaling complex. Experiments using Rag A/B knockout MEFs suggest that this amino acid-regulated self-interaction of GPR137B proteins does not require Rag activity, suggesting a possible direct or indirect regulation of GPR137B by amino acids (Fig. 4c and Supplementary Fig 4c). Notably, the interaction between GPR137B and RagA was not amino acid sensitive (Fig. 4a and Supplementary Fig. 4d).

It has recently been reported that Sestrin2 functions as a leucine sensor[37–41]. We used Sestrin1/2/3 triple knockout cells[38] that have increased basal lysosome localization of mTORC1. However, overexpression of GPR137B could further increase mTOR translocation to lysosomes in these cells (Supplementary Fig. 4e), arguing that GPR137B can regulate Rag and mTORC1 independent of the sestrins. We therefore did not further investigate this regulatory pathway.

We next tested whether GPR137B regulates the localization of Rags analogous to Ragulator proteins that anchor Rags to lysosomes. Markedly, increased GPR137B expression did not only increase mTOR translocation but also caused a small but significant increase in RagA localization at lysosomes (Fig. 4d; see Supplementary Fig. 4f for RagC data) while siRNA against GPR137B reduced lysosomal RagA (Fig. 4e) and RagC (Fig. 4f). Knockdown of the Ragulator component LAMTOR2 is included for comparison. When Ragulator expression was reduced, GPR137B did not significantly increase Rag recruitment or mTORC1 activity and co-expressing of GPR137B did not rescue the reduced RagA lysosome localization (Supplementary Fig. 4g, h). Thus, GPR137B interacts with Rags and increases lysosomal Rag localization in a Ragulator-dependent manner. Taken together with our data in Fig. 3, the binding and localization results suggest that GPR137B regulates Rag localization and possibly RagA GTP loading and activity.

GPR137B increases Rag activity to recruit mTORC1

We used the selective binding of mTORC1 to RagA-GTP over RagA-GDP as a measure to determine whether RagA is in the active GTP bound state[4]. Consistent with a role of GPR137B in regulating RagA GTP loading, knockdown of GPR137B inhibits the amino acid-induced interaction between RagA and both mTOR and raptor (Fig. 5a and Supplementary Fig 5a, b) while overexpression of GPR137B increases the interaction between them (Fig. 5b and Supplementary Fig 5c, d). Markedly, at high GPR137B expression levels, the binding of RagA and raptor is increased even in the absence of amino acids, suggesting that overexpression od GPR137B can increase RagA GTP loading even in the absence of amino acids (Fig. 5b and Supplementary Fig. 5c, d).

We next determined whether co-expression of Rag and GPR137B induces synergistic mTORC1 translocation. When we co-expressed RagC[43] together with Lamp1 control, mTORC1 translocation did not significantly increase, suggesting that Rags, at any level, mediate only minimal basal mTORC1 recruitment when amino acids are low (Fig. 5c, d). In contrast, we found synergistic recruitment of mTORC1 when we co-expressed Rag together

with GPR137B (Fig. 5c, right panel, Fig. 5d, blue line; Supplementary Fig. 6a). The strong synergy between GPR137B and Rag expression on mTOR translocation is consistent with a direct regulation of Rags by GPR137B.

To further investigate whether GPR137B causes mTORC1 translocation through promoting Rag GTP loading, we co-expressed GPR137B with wildtype or dominant-negative RagA/C (RagA T21L/RagC Q120L) in RagA/B null MEFs. These RagA/B knockout cells had no mTORC1 translocation when stably-expressing GPR137B alone (Fig. 3b, c), and minimal rescue of mTORC1 translocation when transiently co-expressing wildtype or dominant-negative Rag A/C and Lamp1. In contrast, we observed robust mTORC1 translocation even in the absence of amino acids when we co-expressed GPR137B and wildtype RagA/C, but significantly lower translocation when we co-expressed DN Rag A/C (Fig. 5e and Supplementary Fig. 6b–d). These results support the hypothesis that the level of GPR137B regulates RagA GTP loading and activity.

Photobleaching recovery analysis suggests that GPR137B regulates a cycle of dynamic activation and dissociation of lysosomal Rags

Figure 4d also revealed an unexpected amino acid-triggered reduction in Rag localization at lysosomes. When we compared the kinetics of Rag and mTOR localization, we found that endogenous RagA and RagC dissociated from lysosomes in response to amino acids with kinetics that paralleled the increase in mTOR translocation to lysosomes (Fig. 6a–c). We next made use of previous studies that showed a negative feedback whereby mTORC1-mediated Rag ubiquitination reduces lysosomal localization of mTORC1 after amino acid stimulation[44,45]. Indeed, when we treated amino acid-stimulated cells with rapamycin to inhibit the activity of mTORC1, more mTOR translocated to lysosomes and a greater fraction of RagA and C dissociated from lysosomes (Fig. 6d–f). The anti-correlated kinetics and amplitude of mTOR and Rag localization suggest that recruitment of mTORC1 and dissociation of Rags are connected events.

We next used fluorescence photobleaching recovery analysis to test whether GTP loading of RagA accelerates dissociation of RagA/C from lysosomes. In cells overexpressing fluorescently-tagged wildtype RagC and dominant negative RagA/C, the RagC dissociation rate was slower compared to cells co-expressing constitutively active RagA/C (Fig. 6g, h). This suggests that GTP loading of RagA lowers the affinity of RagA/C for lysosomes and accelerates RagA/C dissociation. Indeed, lysosomal RagC dissociated more rapidly after amino acid stimulation which increase GTP loading of RagA (Fig. 6i). These results are consistent with a recent publication showing Rags cycle on and off the lysosomes depending on their activation state[46]. When we expressed GPR137B in amino acid-starved cells, we found a small but significant increase in RagC dissociation (Fig. 6j, k). Conversely, when we knocked-down GPR137B, there was a small but significant decrease in the RagC exchange rate (Fig. 6l, m). When we expressed GPR137B in Nprl3−/− HEK293E cells where Rags are mostly GTP-loaded[8], there was no statistically-significant difference in the RagC exchange rate from control cells (Supplementary Fig. 6e, f). Taken together, these results suggest that GPR137B accelerates Rag dissociation from lysosome through RagA GTP loading.

Together with previous studies that showed mTORC1 can be active at different cellular locations[47,48], these results suggest that GPR137B regulates Rags in three steps: First by increasing RagA levels at lysosomes, second by promoting activation of lysosomal RagA which recruits mTORC1 to lysosomes for a limited time period, and third by promoting Rag dissociation from lysosomes possibly as an active or activatable cytosolic Rag/mTORC1 complex.

To directly test whether RagC and the mTORC1 subunit raptor can remain bound to each other in the cytoplasm, we co-expressed RagC with a conjugated C1 domain from rat PKCγ protein[49] along with fluorescently-tagged raptor, constitutively-active RagA, and a membrane marker in HEK293T cells. In this in vivo binding assay, phorbolester (PMA) is used to rapidly recruit cytosolic C1-conjugated RagC to the plasma membrane and monitor how much of the putative binding partner raptor is pulled along. Indeed, we observed a concomitant recruitment of raptor (Fig. 7a–c; Supplementary Fig. 7a, b), arguing that Rags and the mTORC1 subunit raptor can be bound to each other in the cytoplasm. Given the finding that inactive Rags do not bind raptor[4,50], and active Rag dissociates from the lysosomes along with mTOR[46], our results suggest that active Rag-mTORC1 complexes diffuse in the cytoplasm after dissociation and that Rag-mTORC1 remains in an active state until Rag is inactivated.

Mutational analysis in human cells and zebrafish provides evidence that GPR137B regulates lysosome morphology through Rag

Both GPR137B and GPR137 HAP-1 knockout cells showed expanded lysosome compartment as measured by larger Lysotracker Green positive puncta (Fig. 8a, b), as well as increased autophagosomes/autolysosomes as measured by increased LC3B puncta per cell (Fig. 8c), similar to Rag or Rag regulator knockouts[23,26,27]. In addition, in both cell lines, the lysosomal localization of endogenous RagA was decreased, similar to the GPR137B knockdown result (Fig. 8e). Nevertheless, mTORC1 translocation to lysosomes was still regulated by amino acids in both knockout cell lines (Fig. 8d and Supplementary Fig. 8a).

To investigate the function of GPR137B in vivo, we focused on four homologs of GPR137B in zebrafish: *gpr137ba, gpr137bb, gpr137c,* and *gpr137*. Of these genes, Gpr137ba is most similar to the human GPR137B protein (Supplementary Fig. 8b, c). The hypothesis that GPR137B activates RagA predicts that there should be phenotypic similarities between *rraga* mutants and mutants in one or more of the four *gpr137* genes. We generated mutants for three of the annotated genes, *gpr137ba, gpr137c,* and *gpr137,* using TALEN-targeted nucleases (Supplementary Fig. 8d). *gpr137bb* was annotated more recently, and we have analyzed its function in transient CRISPR experiments. Our preliminary studies revealed similarities between mutants for *rraga* and *gpr137ba*, but not *gpr137c* or *gpr137* mutants, or wildtype fish injected with CAS9 and guide RNA for *gpr137bb.* We therefore focused additional analyses on the *gpr137ba* mutants.

Zebrafish *rraga* mutants have abnormal microglia with expanded lysosomes[25], so we examined these specialized brain macrophages in *gpr137ba* mutant zebrafish. Microglia in *gpr137ba* mutants had an expansion of the lysosomal compartment, with large clusters of

Lysotracker Red positive puncta, similar to *rraga* mutant zebrafish (Fig. 8h, i). Homozygous *gpr137ba* mutant fish had otherwise normal morphology and were viable as adults (Supplementary Fig. 8e). Microglial cell numbers and markers of autophagy, such as LC3B and p62, were unchanged in *gpr137ba* mutants relative to controls (Fig. 8f–g, Supplementary Fig. 8f).

RagA represses the activity of the key lysosomal transcription factor TFEB[51], and quantitative real-time PCR studies in zebrafish have demonstrated that transcripts of some TFEB targets are significantly upregulated in *rraga* mutant zebrafish[25,52]. The hypothesis that GPR137B activates RagA predicts that TFEB targets will be similarly upregulated in *gpr137ba* mutants. To investigate this possibility, we conducted qRT-PCR on larvae from a cross of $gpr137c^{+/-}; gpr137^{+/-}; gpr137ba^{-/-}$ X $gpr137c^{-/-}; gpr137^{+/-}; gpr137ba^{+/-}$ adults. Individual fish were genotyped for the *gpr137ba* mutation and pooled, so that one pool of siblings was $gpr137ba^{-/-}$ whereas the other pool was $gpr137ba^{+/-}$; mutations in the other genes were randomly segregated between both pools. qPCR analysis revealed that some TFEB target genes were significantly upregulated in the *gpr137ba* mutant pool compared to the control pool (Fig. 8j), providing evidence that *gpr137ba*, similar to *rraga*, represses the activity of TFEB. Although the levels of p62 protein were similar in immunoblot analysis (Supplementary Fig. 8f), *p62 (sqstm1)* is one of the TFEB target genes whose expression was upregulated in *gpr137ba* mutant pool (Fig. 8j). In summary, this analysis revealed some phenotypic similarities between zebrafish mutants for *gpr137ba* and *rraga*, providing evidence that GPR137B regulates the activity of RagA, and as a consequence, the expression of TFEB targets. Together, the cellular effects of these knockouts indicate that GPR137B regulates some aspects of Rag function also in vivo.

DISCUSSION

Our genome-wide siRNA screen identified GPR137B as a regulator of mTORC1 activation and localization. We focused on GPR137B in part because of its homology to GPCRs, since GPCRs are among the most prominent drug targets in clinical use and since mTORC1 and other lysosomal regulatory pathway components have emerged as promising therapeutic targets for cancer and other diseases[53]. GPR137B has two human homologs that we show also localize to lysosomes and regulate mTORC1 translocation (Fig. 2g and Supplementary Fig. 2f, g). When we performed a sequence homology analysis across multiple eukaryotes[54], we found that genes in the GPR137 family have roots in early eukaryotes with GPR137B homologs being present in *Dictyostelium discoideum*, *Monosiga Bervicollis*, many invertebrates and all vertebrates (Supplementary Fig. 8g). Notably, the mTORC1 regulators Rag, Ragulator and GPR137s all have ancient roots but that Ragulator and GPR137s can each individually or both be lost in different evolutionary branches, suggesting that different species may use alternative control mechanisms to regulate Rags and mTORC1.

Our study shows that knockdown and added expression of GPR137B respectively reduces and increases amino acid-triggered mTORC1 translocation to lysosomes and mTORC1 activity. Furthermore, increased expression of GPR137B can activate mTORC1 even under amino acid-starved conditions (Fig. 2f). We provide different lines of evidence that GPR137B regulates mTORC1 through regulation of both the localization and activity of

Rags. First, GPR137B no longer regulates mTORC1 lysosome localization in RagA/B knockout cells (Fig. 3b, c). Second, the binding interaction between RagA-GTP and mTORC1 shows that GPR137B regulates the GTP loading state of RagA (Fig. 5a, b). Third, we show that GPR137B interacts with RagA and increases Rag recruitment to lysosomes (Fig. 4d). We also showed synergistic control of mTORC1 translocation by GPR137B and Rags in amino acid-starved cells, where mTORC1 recruitment increases in parallel with increasing concentrations of both Rags and GPR137B (Fig. 5c–e and Supplementary Fig. 6b) and significant reduction in mTORC1 translocation when dominant negative Rags are co-expressed, suggesting that GPR137B regulates RagA GTP loading without additional rate-limiting factors.

Our study further revealed that, in response to amino acid stimulation, RagA and C dissociate faster from lysosomes along with mTORC1 as a result of RagA GTP loading (Fig. 6). In supports of such a model, we further show that Rags and raptor remain bound to each other while freely diffusing in the cytoplasm (Fig. 7). This is consistent with the interpretation that GPR137B regulates the formation of active Rag/mTORC1 complexes at lysosomes in an activation cycle whereby the activated Rag/mTORC1 complexes later dissociate from lysosomes to potentially activate substrates elsewhere in the cell until Rag is inactivated.

We investigated knockouts of GPR137B in human HAP-1 cells and in developing zebrafish. Previous studies of RagA/B knockouts in mouse and fish showed that cells can compensate and regulate mTORC1 signaling in a lysosome-independent manner when they lose Rags[22,23,25]. However, knockouts of Rags and Rag regulators[23,25–27] showed a marked increase in accumulation of autophagosomes/autolysosomes as well as lysosomal compartment expansion. Similar to Rag mutant cells, our study showed that knockout of GPR137B, or of GPR137, caused an increase of LC3B positive puncta as well as enlarged lysosome compartments in human cells (Fig. 8a–c). Furthermore, similar to RagA mutant fish, lysosomes were expanded in the microglia of *gpr137ba* zebrafish mutants (Fig. 8h–i), and targets of the lysosomal transcription factor TFEB, which is repressed by RagA, are upregulated in *gpr137ba* mutant zebrafish (Fig. 8j). Together, these results suggest that GPR137B knockout has overlapping cellular and physiological effects with knockouts of Rag A/B and of two Rag regulators, consistent with the interpretation that GPR137B has a cellular and organismal function to regulate Rags.

Finally, GPR137B is to our knowledge unique in that its expression can increase both Rag and mTORC1 localization to lysosomes even in the absence of amino acids, and regulate a dynamic cycle of RagA activation and lysosome dissociation. Given the key roles of mTORC1 signaling in many cancers, it is interesting that a few reports, without providing molecular mechanisms, have suggested a link from GPR137 and GPR137B to different types of cancers[55–58]. Together with our mechanistic results on GPR137B's role in Rag and mTORC1 regulation, this suggests that the three human GPCR-like GPR137 genes are potential therapeutic targets for cancers that depend on RagA and/or mTORC1 signaling for growth and survival.

Materials and Methods

Cell Lines

HS68 primary fibroblast, HeLa, and HEK293T cells were obtained from ATCC. CRISPR-Cas9 edited HAP-1 cells were purchased from Horizon Discovery. RagA/B knockout and parental MEFs were kindly provided by Dr. Kun-Liang Guan's lab. sgNprl3 and parental HEK293E cells, sgSestrin1/2/3 and parental HEK293T cells were kindly provided by Dr. David Sabatini's lab.

Immunofluorescence

Cells were fixed in 4% formaldehyde in PBS for 30 minutes at RT, washed with PBS followed by 15 minutes of 0.2% Triton X-100 permeabilization on ice. 3% BSA in 1xPBS was used for blocking 30 minutes at RT. Primary antibodies were added overnight at 4°C (Hoechst and fluorescent secondary antibodies were added post washing for 1 to 2 hrs at RT). Images were taken either with a 20X air objective, an automated inverted epifluorescence microscope (ImageXpressMicro, Molecular Devices), with a 40X or 100X oil objective on a confocal microscope (Leica TCS SP2 AOBS or 3i imaging system). See section on Fixed/live cell imaging for more detailed description. See Supplementary Table 5 for antibody information.

Zebrafish lines and maintenance

Tupfel long-fin (TL) strain of Danio rerio was used for all zebrafish experiments. All work with zebrafish was conducted with approval from the Stanford University Institutional Animal Care and Use Committee. Embryos and larvae were treated with 0.003% 1-phenyl-2-thiourea (PTU) to inhibit pigmentation, and anesthetized with 0.016% (w/v) Tricaine prior to experimental procedures.

Genome-wide siRNA screen and hit selection

The primary screen was performed using human primary foreskin fibroblasts (HS68 cells). Serum was removed to maximize the amino-acid-induced signal. Cells were stimulated after amino acid removal with a 1 x mixture of all amino acids without glutamine (Figure 1b, schematic). An siARRAY whole human genome siRNA library from ThermoFisher Scientific (Formerly Dharmacon, Cat#G-005000–025), containing 21,041 siRNA pools in 267 X 96-well plates, 80 siRNA pools/plate, was screened using a 384 well formatted assay. Three replicates of each mother siRNA plate were tested at 10 nM concentration in the primary screen; a total of 204 384-well plates. All transfections were done using a Vprep (Velocity 11) with a 96 tip disposable tip head. Lipofectamine 2000 addition and cell addition were done with a Wellmate Dispenser (Matrix). All washing steps, including serum-starvation and amino acid starvation were done using the Plate Washer (Bio-TEK). Hs68 cells were reverse-transfected and the transfection mix was removed 18 hrs to 24 hrs later. Cells were then serum-starved with DMEM/0.1% BSA to keep cell numbers consistent among wells. 68 to 72 hours post transfection, cells were amino acid starved in 1.5% BSA/DPBS for 3 hours and re-stimulated with an amino acid mixture (1xAA) prepared from diluting 50X Essential amino acids and 100X non-essential amino acids in 1.5% BSA/

DPBS. Cells were fixed and stained with an antibody against rpS6 phosphorylated at 240/244. Phosphorylation of rpS6 was imaged with an automated microscope (Axon, Molecular Devices) and integrated fluorescence intensity was quantified using CellProfiler[59].

Primary screen analysis

Using automated fluorescence imaging and automated analysis of antibody staining, we averaged the integrated single-cell rpS6 phosphorylation intensities across all cells in a single well. The mean rpS6 phosphorylation intensity for each well was calculated as the deviation from the median of the surrounding 20 wells in the 384-well plate, in order to minimize regional plate artifacts. The standard deviations of the three replicates of each siRNA treatment (each plate was assayed in parallel in triplicate) were used as a measure of experimental variability[60,61]. The region-corrected means were normalized to the average of the triplicate standard deviations for the entire plate to generate a Z-score = (X-mu)/sigma. The parameter mu was estimated using regional median and the sigma parameters using replicates in each triplicate set. A comparison to nearby 20 wells was used since the library is not randomly organized. Z-scores were normalized to the median Z-score of positive controls (siRheb or siTSC2 controls) in each triplicate set. The resulting fold-change values were used to create a rank-ordered list of genes, and the top 750 genes were selected as hits. An additional list of hits (with a minimum Z-score of 2) was selected based on an additional criterion of matching functional identifiers or literature data (for example: kinase, exchange factor). With these added hits, a total of 1231 genes were selected for further analysis.

Deconvolution of siRNA pools

Using the same assay as in the primary screen, each single siRNA of the 1231 selected pools was tested separately again in a 384-well formatted assay (4 siRNAs targeting the same gene in each pool). Each siRNA was transfected at 10 nM concentration. A quadrant of each plate was filled with siRNA targeting a scrambled sequence (negative controls). The mean integrated phospho-rpS6 intensity for each well was region-corrected by subtracting the average of the mean phospho-rpS6 intensities of the negative controls in a 22-well neighborhood, and then divided by the standard deviations of the mean phospho-rpS6 intensities of all the negative control wells on the same plate. The generated Z-scores were then averaged across duplicates. For each of the original 1231 pools, the deconvolution score was calculated as the average of the 2nd and 3rd strongest single siRNAs. We averaged the 2nd and 3rd strongest siRNA since we noticed a tight correlation between the 1st siRNA and the primary screen pool value (Supplementary Fig. 1c, left), which argued that the strongest siRNA largely recapitulates the screen phenotype. This also means that the averaged 2nd and 3rd hit can provide a second independent test for off-target effects (Supplementary Fig.1c, right). The resulting rank-ordered list of deconvolution scores was at the end manually pruned (removing high-scoring genes with functions likely unrelated or indirectly related to mTOR signaling, such as secreted or extracellular proteins and adding a few lower-scoring genes with relevant functional characteristics) to generate a total of 427 deconvolution hits that we further investigated.

mTOR translocation screen

The 427 hits were then assayed for their effect on mTOR translocation. The single siRNA with the strongest phospho-rpS6 phenotype for each hit (see deconvolution assay above) was tested in duplicate in 96-well format at a concentration of 5 nM and assayed in parallel on a single plate for phospho-rpS6. Cells were reverse-transfected using the same conditions as the primary screen except both the transfection and the assay were performed manually using multichannel pipettes. Cells were starved of amino acids for 4 hours in 1.5% BSA/DPBS and re-stimulated with cycloheximide for 5 minutes (mTOR translocation) or 30 minutes (rpS6 phosphorylation). The plates were fixed and stained with antibodies against mTOR and Lamp2 or phospho-rpS6 (240/244). The correlation coefficient between the intensity of segmented puncta in the mTOR and Lamp2 channels was calculated for each well and averaged across duplicates. A Z-score for mTOR translocation was generated by subtracting the plate median and normalizing the result by the plate standard deviation. A Z-score for the parallel phospho-rpS6 experiment was generated by subtracting the mean of the negative control wells (scrambled siRNA) and normalizing the result to their standard deviation. The plate median was not used in this case because all the genes were expected to perturb phospho-rpS6 levels to some extent, having been selected as deconvolution hits in the first place. Hits with a translocation Z-score below −1.8 and rpS6 phosphorylation below −1.6 were considered for further analysis.

Bioinformatics

Ingenuity Systems pathway analysis (www.ingenuity.com) was used to identify enriched pathways and draw networks. The subset of hits solely chosen based on rank selection were uploaded into Ingenuity pathway analysis and the most enriched canonical pathways/diseases were identified. Fisher's exact test was used to calculate a p-value.

Cell culture and reagents

HS68 primary fibroblast, HeLa, MEFs and HEK293T cells were cultured in 10% FBS/DMEM/PSG (Gibco) medium. HAP-1parental and knockout cells generated by CRISPR-Cas9 were purchased from Horizon Discovery and cultured in 10% FBS/IMDM. Lipofectamine 2000, DPBS media used for starvation, 50X Essential amino acids and 100X non-essential amino acids were obtained from Life Technologies. BSA, cycloheximide, and Phorbol 12-myristate 13-acetate (PMA) were from Sigma-Aldrich. Triton X-100 was from Sigma and 16% formaldehyde was from Ted Pella. n-Octyl-β-D-Glucopyranoside was from Affymetrix. GeneSilencer (Genlantis) was used for siRNA and plasmid co-transfection in HeLa cells. Fugene 6 and X-tremeGENE HP (Roche Applied Science) were used for plasmid transfection into HeLa and HEK293T cells. Lipofectamine 2000 was used to transfect DNA or siRNA into HS68, and HEK293T cells. MEF2 Nucleofector kit was purchased from LONZA to electroporate MEFs using the Amaxa Nucleofector. Rapamycin was purchased from Calbiochem. Torin was purchased from Tocris. Amino acid starvation medium (DMEM without amino acids) was purchased from Athena Enzyme Systems as a custom media. DMEM culture media were used as amino acid add-back medium. Amino acid starvation experiments in screen and FRAP experiments were conducted in 1.5% BSA/DPBS and re-stimulated with an amino acid mixture (1xAA) added to the starvation media.

DMEM without amino acids and 10% dialyzed FBS was used as starvation media for all other experiments.

GPR137B reagents and various mTORC1 reagents

siRNAs against GPR137B were purchased from Dharmacon as 4 separate duplexes. The sequence with the strongest effect was GGACUAAAGUAUUCCACAA (3'UTR); the second strongest was GCAAUAAUGUAGACUGAUA (3'UTR). siRNAs against LAMTOR2 and LAMTOR3 were purchased from Dharmacon as siGenome Smartpools. cDNAs encoding GPR137 (NM_001170880) and GPR137C (NM_001099652) were purchased from Open Biosystems, now part of GE Healthcare. GPR137B cDNA was obtained from in house human ORFeome collection. All GPR137, B and C fluorescently-tagged proteins were cloned by recombining the cDNA into Gateway destination vectors. Wildtype Venus-RagC, Turquoise-RagC, and Venus-RagA were generated by cloning human ORFeome cDNA into Gateway destination vector. The LC3-GFP (Plasmid #24920), Rat Lamp1-mRFP-2xFLAG (Plasmid #34611) and YPF-raptor (Plasmid #73385) were obtained from Addgene. Lamp1-Turquoise was subcloned from Rat Lamp1-mRFP-2xFLAG using Gateway destination vectors. pRK5-HA GST RagA 66L(Addgene plasmid # 19300) and pRK5-HA GST RagA 21L(Addgene plasmid # 19299) were gifts from Dr. David Sabatini. YFP-RagC T75N, CFP-RagC Q120L and CFP-RagA T21N were gifts from Dr. Won Do Heo. NPC1-YFP-2xFLAG was a gift from Dr. Manny Lopez. GPR137B-3xFLAG and Rat Lamp1–3xFLAG were subcloned into pPBbsr2-IRES-Blasticidin and GPR137B-HA was subcloned into pLV-EF1a-IRES Puromycin vector using Gibson assembly (New England Biolabs). C1-mRuby-RagC was generated from Gibson assembly using C1-YFP and mRuby-T-Plastin and subcloned into a Gateway destination vector with wildtype RagC. iRFP-CAAX was generated by PCR of iRFP with primers encoding the CAAX sequence and entry into pLenti-IRES-Puro and also Clonetech C1 vector. HEK293T cells stably expressing GPR137B-3xFLAG and Lamp1–3xFLAG were generated using PiggyBac transposon system (System Biosciences). GPR137B-HA stable cell-line was generated by lentivirus infection. Positive clones were selected using indicated antibiotics.

Fixed/ live-cell imaging

High Resolution images (Fig. 1d, 2b, c, e) were acquired on a scanning confocal system (Leica SP2-AOBS) using a 40× 1.25 NA oil immersion objective. Lower resolution images (Figs. 2g, l, 3a–b, d, 6b, e and Supplementary Figs. 2f, 3a) were acquired on a fully automated fluorescence microscope (ImageXpress Micro XL, Molecular Devices) with a Sola Light Engine (Lumencor), a Zyla 5.5 sCMOS camera (Andor) and using a 20× 0.45 NA Plan Fluor objective (Nikon) with no binning. A 4× 0.13(NA) objective with no binning was used for Figure 1b. FRAP images, plasma membrane translocation images and Lysotracker Green images (Figs. 6g, 7a–b, 8a, and Supplementary Fig. 7a–b) were acquired on an automated widefield/Yokogawa spinning-disc confocal fluorescence microscope system (Intelligent Imaging Innovations, 3i), using either a Nikon 40× 1.3NA oil objective or an 100×1.4NA oil objective, a 3i laser stack (405, 442, 488, 514, 561, 640 nm), a 3i 'Vector' photomanipulation device, an epifluorescence light source, (Sutter Lambda XL), a Yokogawa CSU-W1 scanning head with dual camera port, and two sCMOS cameras (Andor Zyla 4.2). These experiments were performed inside an environmental chamber (Haison).

FRAP experiments (Fig. 6g–l) were either carried out using 40x oil objective at 2×2 binning with epifluorescence light source, or 100xoil objective at 2×2 binning (Supplementary Fig. 6e). A 515nm laser was used for photobleaching and images were acquired at 10s per frame in CFP and YFP EPI channels after photobleaching. Plasma membrane translocation images (Figs. 7a–b and Supplementary Fig. 7a–b) were acquired in confocal mode using 100x oil objective at 2×2 binning and 514nm, 561nm, and 640nm lasers. Lysotracker Green images (Fig. 8a) were acquired using 40xoil objective and 405nm and 488 nm lasers.

Analysis of lysosome localization of mTOR

Fluorescence imaging of mTOR translocation was based on immunostaining using anti-mTOR and anti-Lamp2 antibodies. For screening analysis of the 427 genes, a custom-written MatLab script was used to cross-correlate the mTOR and Lamp2 signals in a perinuclear region as a measure for relative co-localization (Fig. 1e, 2d). A more quantitative mTOR localization and translocation parameter (a slower but more automated analysis) was developed for remainder of the figures (See Supplementary code 1). In this analysis, we identified local Lamp2 positive vesicles and created a binary lysosome mask. We used this mask to subtract a local background for the analysis of mTOR localization and translocation. More specifically, the analysis started by first segmenting nuclei and calculating a distance matrix of the closest cytoplasmic pixels to the nucleus. We used a ring identified by >8 pixels and <20 pixels away from the nucleus as the perinuclear region in which we identified Lamp2 positive vesicles and measured mTOR intensity at these Lamp2 positive sites. The binary mask of Lamp2 puncta was identified by finding the peak intensity values after subtracting non-lysosomal background. This Lamp2 puncta segmentation was then used to measure the relative intensity of pixels in the mTOR channel above background. As the lysosomal regions are a small fraction of the area, we used a shifted mask (several pixels shifted in different directions) to measure and subtract a randomized background to detect a lysosomal mTOR intensity over the averaged background value. The mTOR pixel values in the Lamp2 puncta per cell were averaged to derive a ‘relative translocation score’ for that cell (Figures 2f, Supplementary Fig. 2b, c and remainder of the figures). To quantify levels of RagA, C and Lamp1 at the lysosome (Fig. 6a–f), we substituted RagA, C and Lamp1 for mTOR staining and used an identical automated analysis. For each experiment, 12–25 sites per 96-well were imaged and at least 1,000 cells were analyzed per well and 2–4 wells were included per independent experiment. Statistical analysis was performed either by comparing the averages of control vs. treated wells over independent experiments (Figs. 2f, 2h, 2j, 3c–e, 4e–f, 6a, d, k, m, 7c, 8b–e, 8i–j and Supplementary Fig. 1e, 2a–d, h, j, 4e, g, 6e–f) or comparing averages of transfected cells vs. that of non-transfected cells in the same well (Figs. 2k, 4d, Supplementary Fig. 2h–i, 4f, h). Parametric, two-tailed Student’s t-test and one-way ANOVA analysis followed by Tukey’s test were used as indicated in the figure legends.

Synergy heatmap analysis of Rag and GPR137B

For Figure 5c, HeLa cells were amino acid starved for 10–12hrs, and cells co-expressing Lamp1-Turq and Venus-RagC (n=14004) or GPR137B-Turq and Venus-RagC (n=14207) were binned into 10 equal bins of Turquoise intensities and Venus intensities. Average of mTOR translocation score for each bin is plotted as a blue-yellow heatmap scaled from 50–

450. Gray indicates bins where there was insufficient number of cells. For Figure 5e, RagA/B −/− MEFs transiently co-expressing either Lamp1-Venus with wildtype HA-RagA/ Turquoise-RagC (n=40061) or dominant negative HA-RagA /CFPRagC (T21L/ Q120L) (n=32958), or GPR137B-Venus with wildype HA-RagA/Turquoise-RagC (n=37520) or dominant negative RagA/CFP-RagC (n=38902). We first corrected for fluorophore differences between Turquoise and CFP before generating the heatmaps. We correlated RagA protein levels to RagC fluorescence intensities in the same cell and then normalized dominant negative RagC intensity values by the ratio of the correlation slopes to adjust them to reflect the same amount of RagA proteins at the same wildtype RagC intensities. We plotted all the single-cell measurements for Rag intensity, Lamp1/GPR137B intensity, and mTOR translocation score and selected a range that represented most values in the histograms. RagC and Lamp1/ GPR137B fluorescence intensities were binned into 10 equal bins and average mTOR translocation score each bin is plotted as a blue-yellow heatmap scaled from 0–200. Identical correction and analysis was used for a repeat of this experiment in Supplementary Figure 6b. n=31157for Lamp1 and wildtype RagA/C, and n=201168 for GPR137B and wildtype RagA/C in Supplementary Figure 6b.

FRAP experiments and analysis

All photobleaching experiments were conducted on the 3i imaging system using an 40x or 100x objective (Supplementary Fig.6e, f). Images were acquired every 10s and bleaching was set to the 6^{th} frame. Bleaching was set in 515nm for 1s one time in a rectangular area. For fluorescence recovery measurements, selected lysosomes were tracked manually in ImageJ using Lamp1-Turquoise or GPR137B-Turquoise as a lysosome mask and corresponding average RagC intensity was recorded for each frame. A background region containing no cells was first subtracted from the raw intensities and then divided by a neighboring non-bleached region. All values were then normalized to the frame immediately before bleaching (5^{th} frame). For bar graphs in Figure 6k and m, we derived a single measurement by subtracting the fluorescence intensity at frame 10 from frame 5 to represent the relative recovery for each recovery curve, and then averaging the relative recovery for all curves.

Transfection and starvation of HEK293T for co-immunoprecipitation

One day prior to DNA transfection, cells were plated on collagen coated dishes. Next day, GPR137B was transfected using Lipofectamine 2000 (Thermo Fisher Scientific) in Opti-MEM 1 (Thermo Fisher Scientific) overnight. Media was changed to 10% FBS containing DMEM (Thermo Fisher Scientific). Cells were harvested 48 hours after transfection. For all co-IP experiments, cells were starved and added-back for amino acid in DMEM supplemented with dialyzed FBS. When phosphorylation of S6K was examined (Fig. 2m), DMEM without FBS was used.

Cell Lysis and Immunoprecipitation

For amino acid regulated binding, cells were amino acid starved for 2 hours then amino acids were added back for 10–15 min. Cells were incubated with 1 mg/ mL Dithiobis [succinimidyl propionate] (DSP) for 20 minutes at room temperature then the reaction was quenched by treating cells with 100 mM Tris pH 8.5 for 10 minutes. Cells were lysed in

Octyl-glucoside lysis buffer (60 mM n-Octyl-β-D-Glucopyranoside, 50 mM HEPES [pH 7.4], 150 mM NaCl, and protease inhibitor cocktail (Thermo Fisher Scientific) then homogenized with 25-gauge needle and centrifuged at 1100 x g at 4˚C for 5 minutes to remove nuclei. 0.1% SDS was added to the supernatant. The lysate was sonicated briefly; then incubated at 4˚ C for 1 hour followed by centrifugation at 20,000 x g for 60 minutes. The lysates were adjusted to total protein concentration of 0.1 – 0.2 mg/ml and incubated with the FLAG-M2 affinity gel (Sigma Cat#8823) or mouse anti-HA (Pierce Cat#88837 Lot#QJ224632) at 4˚C overnight. The beads were washed three times with ice-cold lysis buffer with 300 mM NaCl then washed twice with lysis buffer. Immunoprecipitated proteins were denatured in urea containing-SDS sample buffer (final concentration of 62.5 mM Tris-HCl, 12.5% Glycerol, 0.01% Bromophenol, 300 mM DTT, 4 M Urea and 3% SDS) at 37˚C for 30 minutes with rotation. The samples were loaded on 4–12% NuPAGE Bis-Tris, 3–8% Tris-Acetate precast gels, or Bolt 4–12% Bis-Tris Plus gels (Life technologies). The signal intensities were analyzed by ImageJ (NIH) and graphed using Prism (GraphPad).

GPR137B-FLAG and GPR137B-HA co-immunoprecipitation

In order to observe amino acid sensitive GPR137B-GPR137B self-interaction, GPR137B-FLAG and GPR137B-HA were stably co-expressed in RagA/B−/− MEFs or control MEFs at low levels. To achieve this, upstream ORF of pPBbsr2-GPR137b-FLAG and pLV-EF1a-GPR137B-HA were attenuated by engineering to TTT[62]. Only earlier passages of cells were used.

MEFs were amino acid starved for 3–4 hours and re-stimulated for 20 min then DSP crosslinked. GPR137B complex was immunoprecipitated using FLAG-M2 affinity gel at 4˚C overnight. The complex was analyzed by western blot.

TALEN and CRISPR targeting to generate mutations in zebrafish GPR137B homologs

The TAL Effector-Nucleotide Targeter 2.0[63,64] webtool was used to design a pair of transcription activator-like effector nucleases to target *gpr137c, gpr137, and gpr137ba*. The Golden Gate cloning protocol for creating the TALEN plasmids was used[65]. Plasmids were then transcribed using Sp6 mMessage mMachine Kit by Ambion. 400ng of mRNA were injected into 1-cell stage wildtype TL embryos, which were raised to adulthood. To identify founders carrying a null mutation in the germline, we crossed injected fish to wildtype (TL strain) and genotyped a subset of the progeny at 2–3 dpf. The TALEN lesions were given the following names and genotyped using the following primers and restriction assays: ***gpr137c, st117,*** 10bp deletion, forward primer: ttggataagtcggcgtgatag, reverse primer: cgtcctcagagcagaccag, restriction assay using DpnII; ***gpr137, st118,*** 8bp deletion, forward primer: ccatgagcgtcattttcctg, reverse primer: acacccgaatgcatcacac, restriction assay using HpaI; ***gpr137ba, st119,*** 20bp deletion, forward primer: gagcagtgggaagcagaaac, reverse primer: ggtaacgcaaaaccaaccac, restriction assay using: SfaNI. All restriction enzymes cleave the wildtype, but not the mutant allele. Based on the disruption of the restriction site, we identified founders and raised the remaining F1 progeny to adulthood. F1 heterozygous adults for the respective deletions were crossed to the TL strain to establish a stock.

For CRISPR experiments, sgRNAs were designed using CHOPCHOP. The sgRNA was transcribed from the DNA template with T7 polymerase (E2040S, New England Biolabs) and purified using mirVana miRNA isolation kit (AM1560, Ambion). Cas9 protein (Macrolab, Berkeley) and ~300 ng sgRNA were injected into 1-cell stage embryos and embryos were genotyped to detect lesions. The sgRNA used for *gpr137bb* was GGGTCACTACCGGTTGTACC. The efficacy of the sgRNA was determined by sequencing eight individual embryos after PCR using forward primer: GCTATTCCCAGCCACGTGTTC and reverse primer: CACAGGAGATACAGCTCAGTGC

Lysotracker Red and Neutral Red Staining of Live Zebrafish Larvae

Larvae (not selected for gender) at 4 dpf were incubated in a 1:100 dilution of LysoTracker Red DND-99 (Invitrogen) in embryo water at 28.5°C for 45 min, washed twice with embryo water, mounted in 1.5% LMP agarose and imaged with a Zeiss confocal microscope. For the neutral red assay, larvae at 5 dpf (not selected for gender) were incubated in 2.5 μg/ml neutral red at 28.5°C for 2.5 hours, washed twice with embryo water, mounted in 1.5% LMP agarose and analyzed using a dissecting microscope.

Particle Analysis in ImageJ

LysoTracker Red-stained images are thresholded to generate a binary image and despeckled. “Analyze Particles” with a setting of area >30 pixels was used to generate overlays and measure the area of LysoTracker Red stained punctae.

RT-qPCR

Zebrafish larvae were obtained from a cross between *gpr137c+/−*; *gpr137+/−*; *gpr137ba−/−* male X *gpr137c−/−*; *gpr137+/−*; *gpr137ba+/−* female adults. At 5 dpf, larvae (not selected for gender) were anesthetized with tricaine. DNA was prepared from tail fins of individual fish, and the remaining portion of each fish was snap frozen on dry ice. The genotypes of each animal were determined by a PCR assay for the *gpr137ba* lesion and the frozen larvae were pooled based on the genotype for *gpr137ba*. Three batches of 15–16 embryos that were either heterozygous (*gpr137ba+/−*) or homozygous (*gpr137ba−/−*) mutants were pooled separately to obtain biological triplicates. Total RNA was extracted from pooled embryos using the RNAeasy kit (QIAGEN). cDNA was synthesized using iScript supermix (Biorad 1708840). qPCR was performed with SsoAdvancedTM Universal SYBR Green Supermix (Biorad 1725271) on the Bio-Rad CFX384 Real-Time PCR Detection System. All experiments were done in biological and technical triplicates. Transcript levels were normalized to eif1-α (Shen et al., 2016; Shiau et al., 2013). Relative mRNA levels were calculated using ΔΔCT.

Statistics and Reproducibility

Unpaired, parametric, two-tailed Student’s t-tests were performed using Prism (GraphPad) to analyze statistical significance of experiments in Figs. 2f, 2h, 2k, 3d, 4e, 4f, 6m, 7c, Supplementary Figs. 1e, 2c, 2h, 2ji, e and 6f. Paired, parametric, two-tailed Student’s t-tests were used for experiments in Figs. 6d, 6k, Supplementary Figs. 2e, 2g, 4h, and ratio paired t-tests were applied to Figs 2j, 6a, 8b, 8c and Supplementary Figs. 2d and 2i. For multiple

group comparisons, One-way ANOVA analysis was performed using GraphPad for Figs 3c and supplementary Figs. 2b, and repeated measures ANOVA was used for Figs. 4d, 8d, 8e, and Supplementary Fig.4f. All ANOVA analysis was followed by Tukey's test. Unpaired, parametric, two-tailed t-test with Welch's correction was used for fish experiments in Figs. 8g, i and j. Description of each statistical test and P values are included with each experimental source data (Supplementary Table 4). Experiments in Figs. 2l, 2m, 3e, 4a, 4b, 4c, 5e, Supplementary Figs. 1a, 3b, 4a, 4b, 4d, 5a, and 7a are performed two times independently showing similar results. Experiment in Supplementary Fig. 7b was done once. All other experiments were performed three or more times independently showing similar results.

Code availability.

MATLAB script for analysis of lysosomal localization is shared in Supplementary Note.

Supplementary Material

Refer to Web version on PubMed Central for supplementary material.

Acknowledgements:

K.S and H.I were supported by fellowships from A*STAR Singapore and AHA (18POST33990334), respectively. W.S.T. is a Catherine R. Kennedy and Daniel L. Grossman Fellow in Human Biology. Work in the Talbot lab was supported by NIH grant R01NS050223 and NMSS grant RG-1707–28694 and in the Meyer lab by R35 GM127026 and UL1TR001085 and Stanford SPARK Translational Program. We thank Drs. D. Garbett, M. Chung, S. Cappell, S. Spencer, S. Collins, M. Koberlin and other lab members for discussions and critical reading of the manuscript, A. Bisaria for plasmids, Dr. M. Lopez for the NPC1 construct, David Solow-Cordero at the HTBC for help in preparing siRNAs for screening.

K.S. generated TALEN mutations in zebrafish and analyzed microglia. H.I. generated CRISPR mutations in zebrafish and performed qPCR. K.S., H.I., and W.S.T. designed zebrafish experiments, analyzed data, and contributed to writing the manuscript. L.G. and T.M. planned the initial siRNA screen and follow-up experiments characterizing GPR137B function. T.M. supervised the project and wrote most of the manuscript together with L.G. L.G. and T.M. planned and L.G. performed and analyzed all cell-based experiments. A.S., L.G. and T.M. planned and A.S. performed and analyzed all biochemistry studies of GPR137B. K.H. and L.G. performed the initial siRNA screen and R.W. helped with the initial analysis of the screen. A.H. helped with imaging, G.D. with image analysis and evolutionary analysis of GPR137B. X.G. and J.R. helped with some cell biology and biochemical studies.

REFERENCES

1. Hirose E, Nakashima N, Sekiguchi T & Nishimoto T RagA is a functional homologue of S. cerevisiae Gtr1p involved in the Ran/Gsp1-GTPase pathway. J. Cell Sci 111, 11–21 (1998). [PubMed: 9394008]
2. Schürmann A, Brauers A, Massmann S, Becker W & Joost HG Cloning of a novel family of mammalian GTP-binding proteins (RagA, RagBs, RagB1) with remote similarity to the Ras-related GTPases. J. Biol. Chem 270, 28982–8 (1995). [PubMed: 7499430]
3. Sekiguchi T, Hirose E, Nakashima N Ii, M. & Nishimoto, T. Novel G proteins, Rag C and Rag D, interact with GTP-binding proteins, Rag A and Rag B. J. Biol. Chem 276, 7246–57 (2001). [PubMed: 11073942]
4. Sancak Y et al. The Rag GTPases bind raptor and mediate amino acid signaling to mTORC1. Science 320, 1496–501 (2008). [PubMed: 18497260]
5. Kim E, Goraksha-Hicks P, Li L, Neufeld TP & Guan K-L Regulation of TORC1 by Rag GTPases in nutrient response. Nat. Cell Biol 10, 935–945 (2008). [PubMed: 18604198]
6. Sancak Y et al. Ragulator-rag complex targets mTORC1 to the lysosomal surface and is necessary for its activation by amino acids. Cell 141, 290–303 (2010). [PubMed: 20381137]

7. Bar-Peled L, Schweitzer LD, Zoncu R & Sabatini DM Ragulator Is a GEF for the Rag GTPases that Signal Amino Acid Levels to mTORC1. Cell 150, 1196–1208 (2012). [PubMed: 22980980]
8. Bar-Peled L et al. A Tumor suppressor complex with GAP activity for the Rag GTPases that signal amino acid sufficiency to mTORC1. Science 340, 1100–6 (2013). [PubMed: 23723238]
9. Panchaud N, Péli-Gulli M-P & De Virgilio C Amino acid deprivation inhibits TORC1 through a GTPase-activating protein complex for the Rag family GTPase Gtr1. Sci. Signal 6, ra42(2013). [PubMed: 23716719]
10. Efeyan A et al. Regulation of mTORC1 by the Rag GTPases is necessary for neonatal autophagy and survival. Nature 493, 679–83 (2013). [PubMed: 23263183]
11. Ricoult SJH & Manning BD The multifaceted role of mTORC1 in the control of lipid metabolism. EMBO Rep. 14, 242–251 (2012). [PubMed: 23399656]
12. Settembre C et al. TFEB Links Autophagy to Lysosomal Biogenesis. Science (80-.) 332, 1429–1433 (2011).
13. Martina JA & Puertollano R Rag GTPases mediate amino acid-dependent recruitment of TFEB and MITF to lysosomes. J. Cell Biol 200, 475–91 (2013). [PubMed: 23401004]
14. Huang J & Manning BD A complex interplay between Akt, TSC2 and the two mTOR complexes. Biochem. Soc. Trans 37, 217–22 (2009). [PubMed: 19143635]
15. Inoki K, Zhu T & Guan K-L TSC2 Mediates Cellular Energy Response to Control Cell Growth and Survival. Cell 115, 577–590 (2003). [PubMed: 14651849]
16. Potter CJ, Pedraza LG & Xu T Akt regulates growth by directly phosphorylating Tsc2. Nat. Cell Biol 4, 658–665 (2002). [PubMed: 12172554]
17. Linares JF et al. K63 Polyubiquitination and Activation of mTOR by the p62-TRAF6 Complex in Nutrient-Activated Cells. Mol. Cell 51, 283–296 (2013). [PubMed: 23911927]
18. Zoncu R et al. mTORC1 senses lysosomal amino acids through an inside-out mechanism that requires the vacuolar H(+)-ATPase. Science 334, 678–83 (2011). [PubMed: 22053050]
19. Rebsamen M et al. SLC38A9 is a component of the lysosomal amino acid sensing machinery that controls mTORC1. Nature 519, 477–481 (2015). [PubMed: 25561175]
20. Wang S et al. Metabolism. Lysosomal amino acid transporter SLC38A9 signals arginine sufficiency to mTORC1. Science 347, 188–94 (2015). [PubMed: 25567906]
21. Jung J, Genau HM & Behrends C Amino Acid-Dependent mTORC1 Regulation by the Lysosomal Membrane Protein SLC38A9. Mol. Cell. Biol 35, 2479–2494 (2015). [PubMed: 25963655]
22. Efeyan A et al. RagA, but Not RagB, Is Essential for Embryonic Development and Adult Mice. Dev. Cell 29, 321–329 (2014). [PubMed: 24768164]
23. Kim YC et al. Rag GTPases are cardioprotective by regulating lysosomal function. Nat. Commun 5, 4241(2014). [PubMed: 24980141]
24. Averous J et al. Requirement for lysosomal localization of mTOR for its activation differs between leucine and other amino acids. Cell. Signal 26, 1918–1927 (2014). [PubMed: 24793303]
25. Shen K, Sidik H & Talbot WS The Rag-Ragulator Complex Regulates Lysosome Function and Phagocytic Flux in Microglia. Cell Rep. 14, 547–559 (2016). [PubMed: 26774477]
26. Cai W, Wei Y, Jarnik M, Reich J & Lilly MA The GATOR2 Component Wdr24 Regulates TORC1 Activity and Lysosome Function. PLoS Genet. 12, e1006036(2016). [PubMed: 27166823]
27. Soma-Nagae T et al. The lysosomal signaling anchor p18/LAMTOR1 controls epidermal development by regulating lysosome-mediated catabolic processes. J. Cell Sci 126, 3575–84 (2013). [PubMed: 23781028]
28. Ruvinsky I & Meyuhas O Ribosomal protein S6 phosphorylation: from protein synthesis to cell size. Trends Biochem. Sci 31, 342–348 (2006). [PubMed: 16679021]
29. Rosner M & Hengstschläger M Evidence for cell cycle-dependent, rapamycin-resistant phosphorylation of ribosomal protein S6 at S240/244. Amino Acids 39, 1487–92 (2010). [PubMed: 20464435]
30. Beugnet A, Tee AR, Taylor PM & Proud CG Regulation of targets of mTOR (mammalian target of rapamycin) signalling by intracellular amino acid availability. Biochem. J 372, 555–66 (2003). [PubMed: 12611592]

31. Gao J et al. TM7SF1 (GPR137B): a novel lysosome integral membrane protein. Mol. Biol. Rep 39, 8883–9 (2012). [PubMed: 22729905]
32. Chan EY mTORC1 Phosphorylates the ULK1-mAtg13-FIP200 Autophagy Regulatory Complex. Sci. Signal. 2, pe51–pe51 (2009).
33. Bjørkøy G et al. p62/SQSTM1 forms protein aggregates degraded by autophagy and has a protective effect on huntingtin-induced cell death. J. Cell Biol 171, 603–14 (2005). [PubMed: 16286508]
34. Gingras A-C, Raught B & Sonenberg N Regulation of translation initiation by FRAP/mTOR. Genes Dev. 15, 807–826 (2001). [PubMed: 11297505]
35. Miron M, Lasko P & Sonenberg N Signaling from Akt to FRAP/TOR targets both 4E-BP and S6K in Drosophila melanogaster. Mol. Cell. Biol 23, 9117–26 (2003). [PubMed: 14645523]
36. Fingar DC, Salama S, Tsou C, Harlow E & Blenis J Mammalian cell size is controlled by mTOR and its downstream targets S6K1 and 4EBP1/eIF4E. Genes Dev 16, 1472–87 (2002). [PubMed: 12080086]
37. Chantranupong L et al. The Sestrins Interact with GATOR2 to Negatively Regulate the Amino-Acid-Sensing Pathway Upstream of mTORC1. Cell Rep. 9, 1–8 (2014). [PubMed: 25263562]
38. Wolfson RL et al. Sestrin2 is a leucine sensor for the mTORC1 pathway. Science (80-.). 351, 43–48 (2016).
39. Kim JS et al. Sestrin2 inhibits mTORC1 through modulation of GATOR complexes. Sci. Rep 5, 9502(2015). [PubMed: 25819761]
40. Parmigiani A et al. Sestrins Inhibit mTORC1 Kinase Activation through the GATOR Complex. Cell Rep. 9, 1281–1291 (2014). [PubMed: 25457612]
41. Peng M, Yin N & Li MO Sestrins function as guanine nucleotide dissociation inhibitors for Rag GTPases to control mTORC1 signaling. Cell 159, 122–133 (2014). [PubMed: 25259925]
42. Fehrenbacher N et al. The G protein–coupled receptor GPR31 promotes membrane association of KRAS. J. Cell Biol 216, 2329–2338 (2017). [PubMed: 28619714]
43. Oshiro N, Rapley J & Avruch J Amino acids activate mammalian target of rapamycin (mTOR) complex 1 without changing Rag GTPase guanyl nucleotide charging. J. Biol. Chem 289, 2658–74 (2014). [PubMed: 24337580]
44. Deng L et al. The ubiquitination of rag A GTPase by RNF152 negatively regulates mTORC1 activation. Mol. Cell 58, 804–18 (2015). [PubMed: 25936802]
45. Jin G et al. Skp2-Mediated RagA Ubiquitination Elicits a Negative Feedback to Prevent Amino-Acid-Dependent mTORC1 Hyperactivation by Recruiting GATOR1. Mol. Cell 58, 989–1000 (2015). [PubMed: 26051179]
46. Lawrence RE et al. A nutrient-induced affinity switch controls mTORC1 activation by its Rag GTPase-Ragulator lysosomal scaffold. Nat. Cell Biol 20, 1052–1063 (2018). [PubMed: 30061680]
47. Zhou X et al. Dynamic Visualization of mTORC1 Activity in Living Cells. Cell Rep. 10, 1767–1777 (2015). [PubMed: 25772363]
48. Manifava M et al. Dynamics of mTORC1 activation in response to amino acids. Elife 5, (2016).
49. Shen K, Teruel MN, Subramanian K & Meyer T CaMKIIβ Functions As an F-Actin Targeting Module that Localizes CaMKIIα/β Heterooligomers to Dendritic Spines. Neuron 21, 593–606 (1998). [PubMed: 9768845]
50. Gong R et al. Crystal structure of the Gtr1p-Gtr2p complex reveals new insights into the amino acid-induced TORC1 activation. Genes Dev. 25, 1668–73 (2011). [PubMed: 21816923]
51. Napolitano G & Ballabio A TFEB at a glance. J. Cell Sci 129, 2475–2481 (2016). [PubMed: 27252382]
52. Meireles AM et al. The Lysosomal Transcription Factor TFEB Represses Myelination Downstream of the Rag-Ragulator Complex. Dev. Cell 47, 319–330.e5 (2018). [PubMed: 30399334]
53. Xie J, Wang X & Proud CG mTOR inhibitors in cancer therapy. F1000Research (2016). doi: 10.12688/f1000research.9207.1
54. Dey G, Jaimovich A, Collins SR, Seki A & Meyer T Systematic Discovery of Human Gene Function and Principles of Modular Organization through Phylogenetic Profiling. Cell Rep. 10, 993–1006 (2015). [PubMed: 25683721]

55. Wang C, Liang Q, Chen G, Jing J & Wang S Inhibition of GPR137 suppresses proliferation of medulloblastoma cells in vitro. Biotechnol. Appl. Biochem 62, 868–873 (2015). [PubMed: 25524330]
56. Cui X et al. Knockdown of GPR137 by RNAi inhibits pancreatic cancer cell growth and induces apoptosis. Biotechnol. Appl. Biochem 62, 861–867 (2015). [PubMed: 25471990]
57. Andrade VP et al. Gene expression profiling of lobular carcinoma in situ reveals candidate precursor genes for invasion. Mol. Oncol (2015). doi:10.1016/j.molonc.2014.12.005
58. Brunetti M et al. Recurrent fusion transcripts in squamous cell carcinomas of the vulva. Oncotarget 8, 16843–16850 (2017). [PubMed: 28186972]
59. Carpenter AE et al. CellProfiler: image analysis software for identifying and quantifying cell phenotypes. Genome Biol. 7, R100(2006). [PubMed: 17076895]
60. Paulsen RD et al. A genome-wide siRNA screen reveals diverse cellular processes and pathways that mediate genome stability. Mol. Cell 35, 228–39 (2009). [PubMed: 19647519]
61. Galvez T et al. siRNA screen of the human signaling proteome identifies the PtdIns(3,4,5)P3-mTOR signaling pathway as a primary regulator of transferrin uptake. Genome Biol. 8, R142(2007). [PubMed: 17640392]
62. Ferreira JP, Overton KW & Wang CL Tuning gene expression with synthetic upstream open reading frames. Proc. Natl. Acad. Sci 110, 11284–11289 (2013). [PubMed: 23798422]
63. Cermak T et al. Efficient design and assembly of custom TALEN and other TAL effector-based constructs for DNA targeting. Nucleic Acids Res 39, e82(2011). [PubMed: 21493687]
64. Doyle EL et al. TAL Effector-Nucleotide Targeter (TALE-NT) 2.0: tools for TAL effector design and target prediction. Nucleic Acids Res. 40, W117–22 (2012). [PubMed: 22693217]
65. Sanjana NE et al. A transcription activator-like effector toolbox for genome engineering. Nat. Protoc 7, 171–92 (2012). [PubMed: 22222791]
66. Shiau CE, Monk KR, Joo W & Talbot WS An anti-inflammatory NOD-like receptor is required for microglia development. Cell Rep. 5, 1342–52 (2013). [PubMed: 24316075]

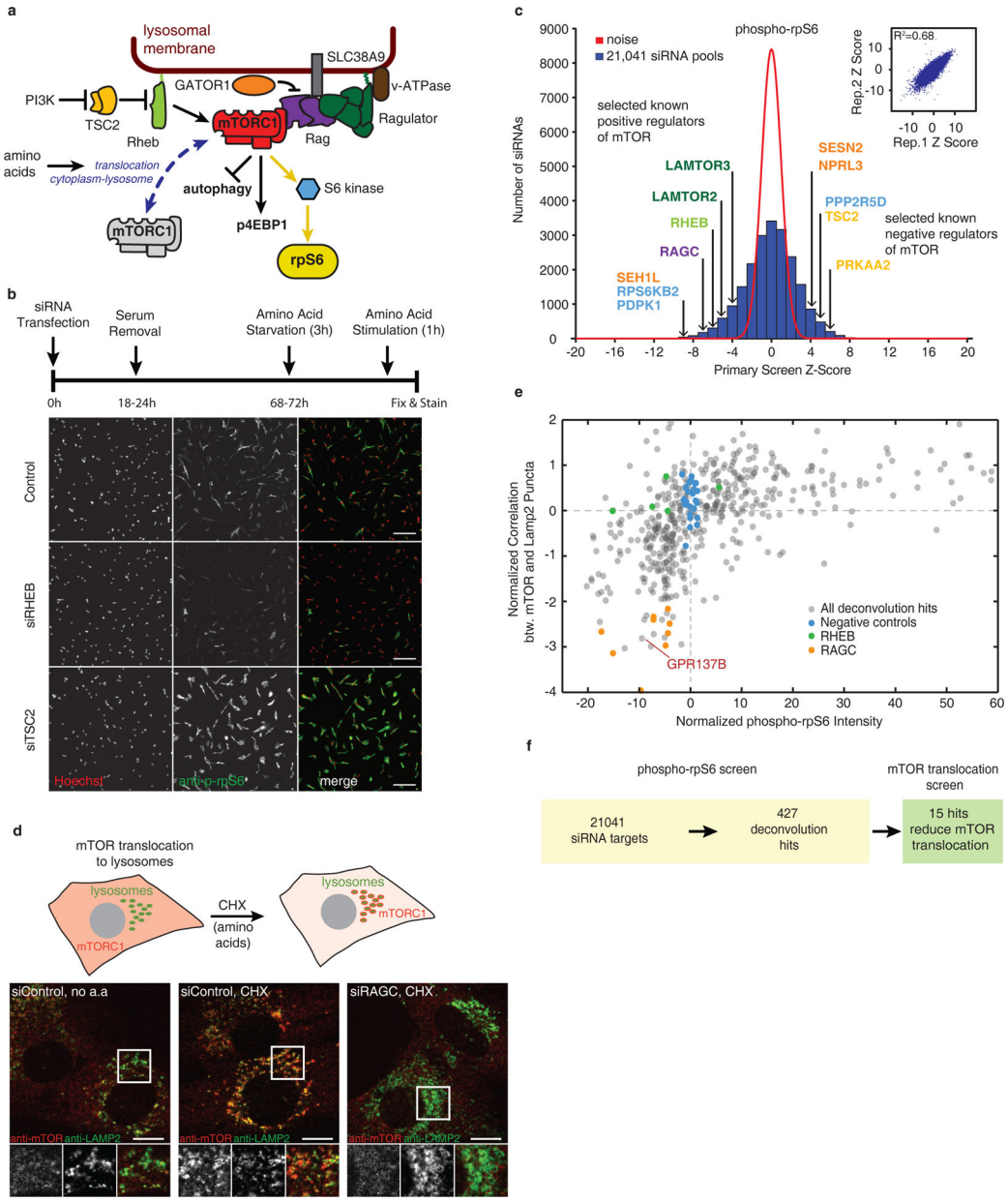

Figure 1: A genome-wide siRNA screen in human primary fibroblasts identifies candidate regulators of amino acid-stimulated mTORC1 translocation and activation

(**a**) Schematic representation of the mTORC1 signaling pathway. rpS6 phosphorylation at 240/244 was used as readout for amino acid-stimulated mTORC1 activation in the siRNA screen. (**b**) *Top*, siRNA screening strategy. *Bottom*, representative immunofluorescence images showing rpS6 phosphorylation at 240/244 in response to amino acid stimulation. Knockdown of the mTOR pathway components Rheb and TSC2 are shown as examples for increased and decreased rpS6 phosphorylation, respectively. Scale bar, 200 μm. (**c**) Genome-wide screen identifies siRNA pools (4 individual siRNAs targeting the same gene) that increase or decrease rpS6 phosphorylation. Z-scores of 21,041 siRNA pools (blue) are plotted over a normally-distributed noise distribution (red). Inset shows reproducibility of Z-scores of two replicate sets, calculated by linear regression. Labeled genes show known

mTOR pathway regulators, color-coded according to the schematic in **a**. (**d**) Microscopy-based mTORC1 translocation assay based on automated correlation between mTOR and Lamp2 images. Confocal images of Hs68 fibroblasts co-stained for endogenous Lamp2 (green) and mTOR (red). Scale bars, 10μm. (**e**) Lysosome translocation screen identifies candidate siRNAs that decrease mTOR localization to lysosomes as well as rpS6 phosphorylation. (**f**) Sequential selection strategy for candidate regulatory genes (See Methods). Experiments in **b** and **d** are repeated independently 12 and 5 times respectively, as controls for each run of the screen.

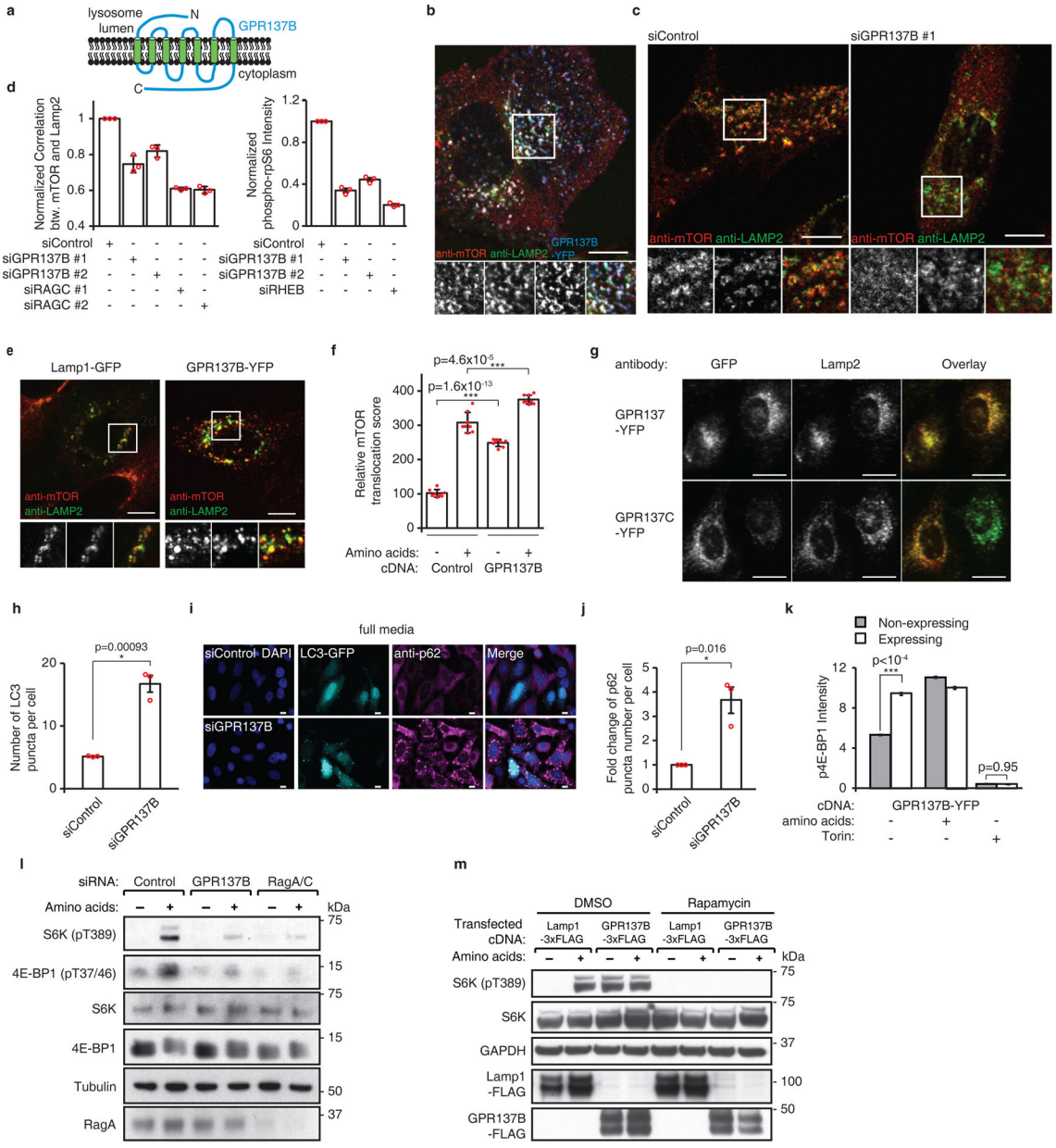

Figure 2: GPR137B regulates mTORC1 translocation to lysosomes and mTORC1 activation

(**a**) Predicted transmembrane domains of GPR137B. (**b**) Confocal images of expressed GPR137B-YFP, lysosome marker Lamp2 and mTOR in Hs68 cells. (**c**) siRNA knockdown of GPR137B reduces amino acid-induced mTOR translocation. (**d**) Analysis of mTOR and Lamp2 co-localization and rpS6 phosphorylation for siRNAs targeting GPR137B, Rheb and RagC. Error bars, ± SD of mean; n=3 independent experiments. (**e**) Confocal images of Hela cells showing increased amino acid-induced mTOR translocation in cells expressing GPR137B-YFP or Lamp1-GFP as control. (**f**) Binary mask analysis showing that amino acid-triggered increase in mTOR localization at lysosomes is regulated by GPR137B-YFP overexpression. Error bars, ± SD of mean, 8 independent experiments, $p=1.6\times10^{-13}$ (two-tailed Student's t-test). (**g**) Lysosome localization of GPR137-YFP and GPR137C-YFP

(HeLa cells). (**h**) siRNA knockdown of GPR137B enhances autophagy as measured by LC3-GFP. Error bars, ± SD of mean; n=3 independent experiments (two-tailed Student's t-test). (**i, j**) siRNA knockdown of GPR137B causes autophagy flux defects as measured by p62 staining. Scale bar, 20 μm. Error bars, ± SD of mean (P value, ratio paired, two-tailed Student's t-test; n=3 independent experiments). (**k**) GPR137B-YFP expression causes phosphorylation of 4E-BP1 during amino acid starvation. Error bars, ± SEM of mean (P values, comparison of transfected, n= 2329 cells, no aa; 2211 cells, plus aa; 2308 cells, Torin; to untransfected cells, n=3256 cells, no aa; 3099 cells, plus aa; 3048 cells, Torin; two-tailed Student's t-test). (**l**) Knockdown of GPR137B inhibits amino acid-induced S6K and 4E-EP1 phosphorylation. HEK293T cells transfected with siControl, siGPR137B, or siRagA/C were amino acid-starved for 1 hour and stimulated w/wo amino acid for 30 min. Western blot analysis of phosphorylation of S6K and 4E-BP1. (**m**) Same as (**l**) but with transiently transfected GPR137B-3xFLAG or Lamp1–3xFLAG. Amino acid starvation for 3 hours and amino acid re-addition for 30 min w/wo rapamycin. Results in **b, c**, **g** were confirmed by 3 independent experiments, in **l** and **m** by 2 independent experiments. In all figures, *, p=0.01 to 0.05; **, p=0.001 to 0.1, ***, p<0.001. All scale bars are 10 μm except when noted.

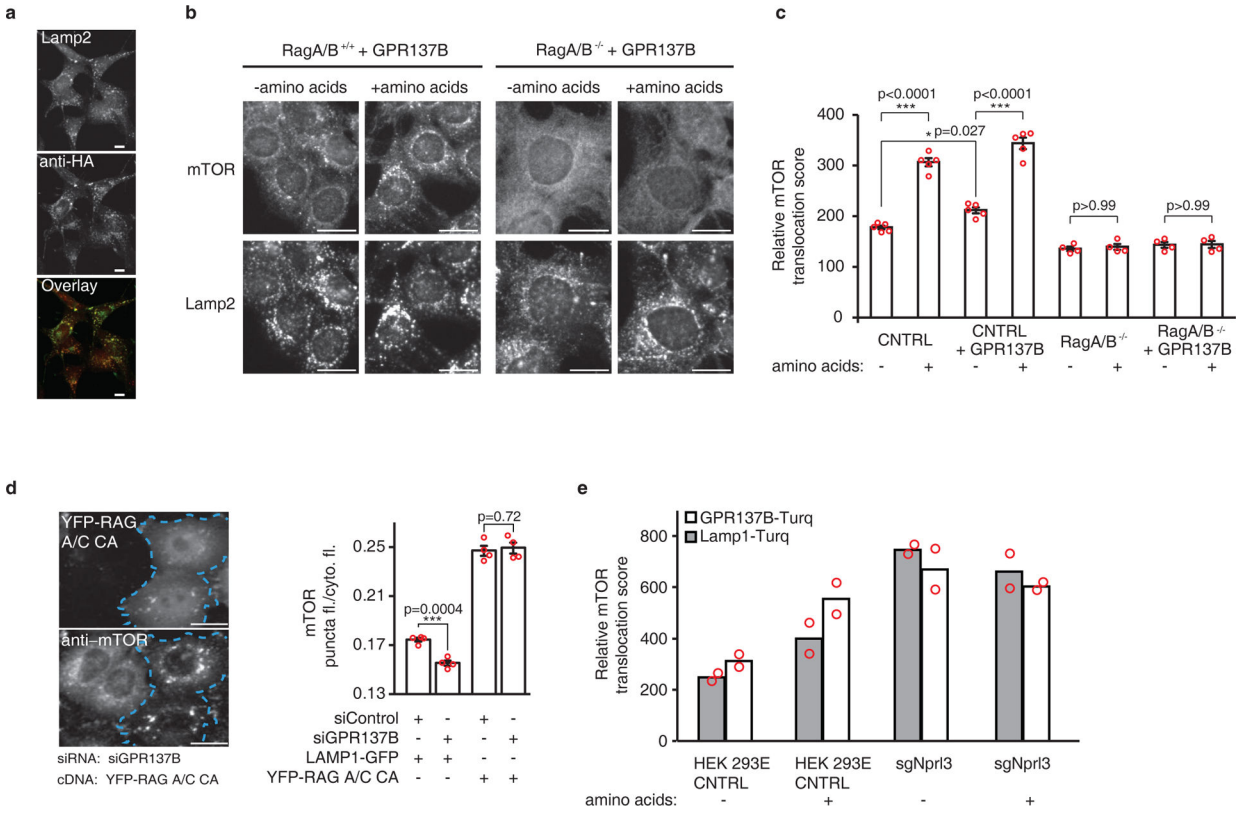

Figure 3: GPR137B regulates mTORC1 through RagA/B

(**a**) Stable expression of GPR137B-HA in RagA/B−/− MEFs visualized by staining for HA and Lamp2. Scale bar, 20 μm. Experiment was performed twice. (**b**) mTOR translocation could not be rescued in RagA/B−/− MEFs by stable expression of GPR137B. MEFs starved of amino acids for 60 min and re-stimulated with amino acids for 10 min were stained for mTOR and Lamp2. Scale bars, 20 μm. (**c**) Quantification of mTOR translocation in RagA/B +/+ and RagA/B−/− MEFs stably expressing GPR137B or not. Error bars are ± SD of population average and One-way ANOVA analysis followed by Tukey's test shows that there is statistical significance among control groups with or without GPR137B, but not among RagA/B−/− MEFs without or without GPR137B ; n=4 independent experiments. (**d**) Expression of constitutively active RagA/C heterodimer (RagAQ66L/T75N) rescued mTOR translocation in cells treated with siGPR137B. *Left*, HeLa cells transfected with GPR137B siRNA and RagAQ66L/ RagCT75N (YFP-RagA/C CA) then stained for mTOR. Cells co-expressing YFP-RagA/C CA are marked by blue-dashed lines. *Right*, Analysis of effects on mTOR translocation by Lamp1-GFP or YFP-RagA/C CA expression in cells treated with siGPR137B versus siControl. Error bars are ± SD of population average and P value is calculated using two-tailed Student's t-test; n=4 independent experiments; Scale bar, 20 μm. (**e**) GPR137B does not induce additional mTOR translocation in Nprl3−/− HEK293E cells that have constitutively active RagA. Parental HEK293E cells or Nprl3−/− cells transfected with either Lamp1-Turquoise or GPR137B-Turquoise were treated as in **a**. Mean from n=2 independent experiments is plotted

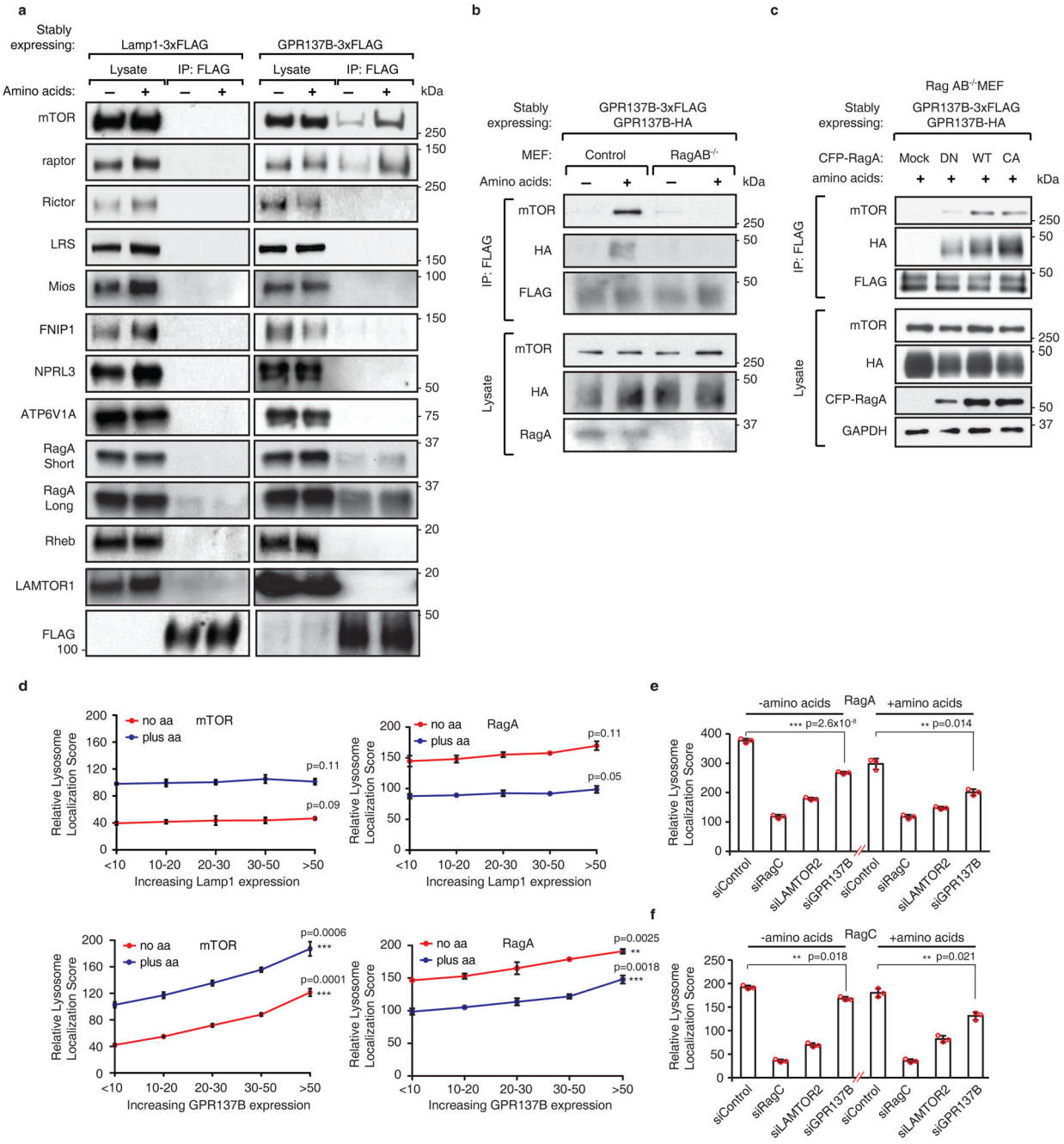

Figure 4: GPR137B forms an amino acid sensitive complex with mTORC1 through Rag GTPases and binds RagA constitutively as an adaptor for lysosomal localization

(**a**) Amino acid-regulated interaction of GPR137B with mTOR, raptor and RagA. HEK293T cells stably expressing Lamp1- or GPR137B-3xFLAG, amino acid-starved for 2 hours, stimulated for 10 min. (**b**) Rag GTPases are necessary for the GPR137B–mTOR interaction & evidence of self-interaction between GPR137Bs. GPR137B-3xFLAG and GPR137B-HA were stably expressed in control or RagA/B−/− MEFs. (**c**) RagA overexpression restores GPR137B self-interaction regardless of RagA GTP loading. RagA DN(T21N), WT or CA(Q66L) mutants were expressed in RagA/B−/− MEFs. Cells were amino acid starved for

4 hours then stimulated for 20 minutes. For **a**, **b**, **c**, n=2 independent experiments. (**d**) Amino acid stimulation reduces lysosome localization of RagA and GPR137B increases RagA localization at lysosomes. Increasing expression of GPR137B causes gradual increase in lysosome localization of mTOR, *left*, as well as of RagA, *right*. Amino acid-starved or re-stimulated HeLa cells expressing either Lamp1-Turquoise or GPR137B-Turquoise were stained for endogenous mTOR or RagA and Lamp2, and binned for different levels of Turquiose expression. The median value for each bin is plotted as mean of triplicates ± SD from 3 independent experiments. Repeated measures One-way ANOVA analysis and followed by Tukey's test shows statistically significant differences among different expression bins of GPR137B but not Lamp1. (**e, f**) Knockdown of GPR137B decreases lysosomal localization of RagA in **e** and of RagC in **f** in amino acid-starved and re-stimulated HeLa cells. Two-tailed, Student's t-test shows statistically significant difference between control and siGPR137B. Mean ±SD is plotted from n=3 independent experiments.

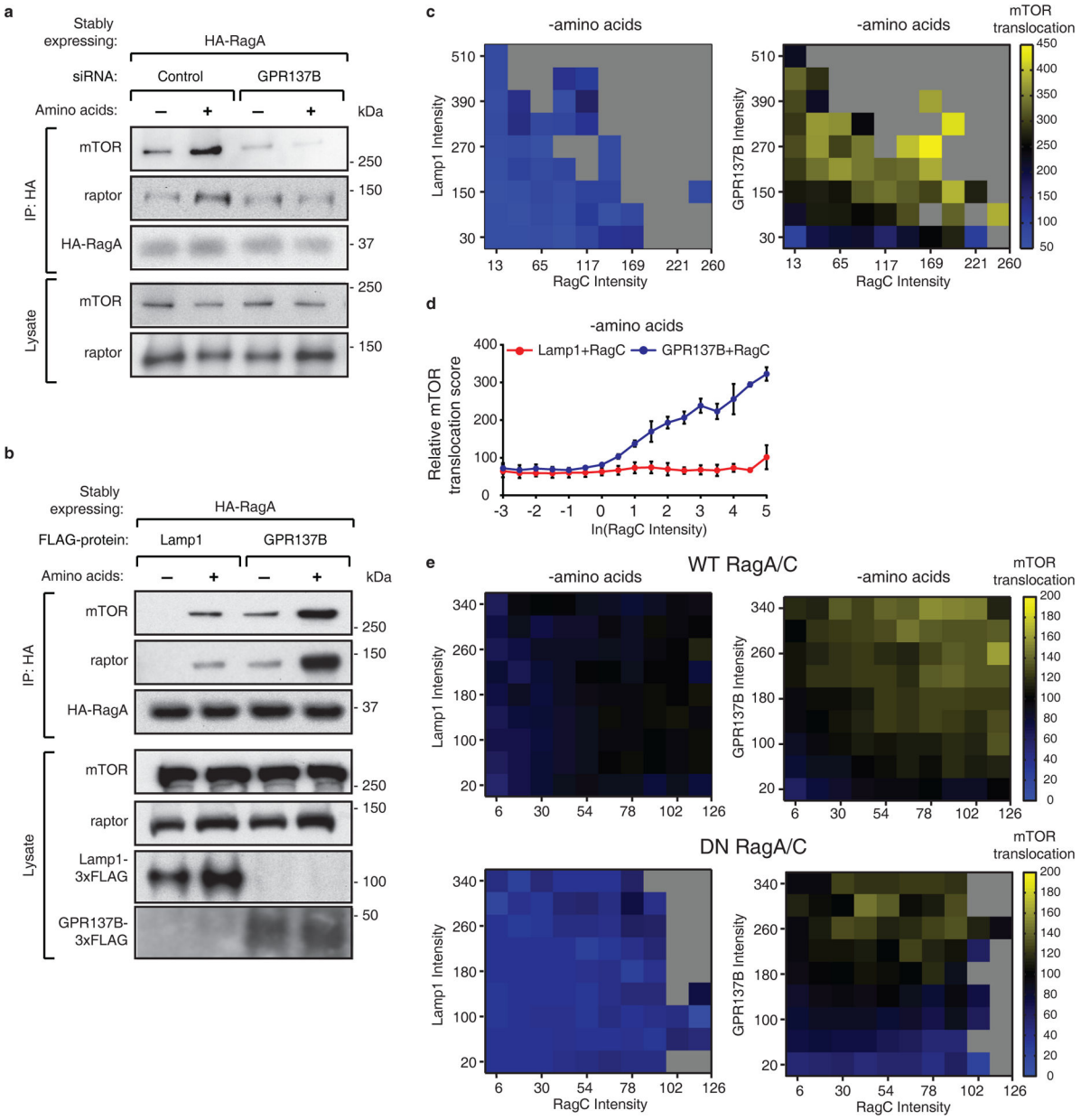

Figure 5: Evidence that GPR137B can activate Rag A/C even in absence of amino acids

(**a**) mTORC1 interaction with HA-RagA was markedly reduced in cells treated with siGPR137B. GPR137B was knocked down in HEK293T cells stably expressing HA-RagA. HA-RagA was immunoprecipitated and the interaction with endogenous mTORC1 subunits was detected by Westernblot. (**b**) mTORC1 interaction with HA-RagA was increased in GPR137B overexpressing cells. GPR137B was transiently overexpressed in HEK293T cells stably expressing HA-RagA. In **a** and **b,** the cells were amino acid-starved for 2 hours then treated with starvation or amino acid-containing media for 10 min. Cells were then treated with a cell-permeable chemical cross-linker (DSP) and subjected to HA immunoprecipitation. n = 2 independent experiments in **a** and **b**. (**c**) Analysis of synergism between GPR137B and Rags for mTORC1 activation. GPR137B co-expression with RagC

promotes Rag expression-dependent recruitment of mTORC1 during amino acid starvation (10–12hrs). Control heatmap experiments show co-expression of Lamp1 with RagC does not induce mTORC1 translocation at any expression level of Lamp1 or RagC (*left*), but co-expression of GPR137B with RagC causes synergistic mTORC1 translocation at even low levels of RagC expression in the absence of amino acids (*right*). Heatmaps are plotted from translocation scores pooled from 3 independent experiments. (**d**) Synergy analysis as in **c** comparing GPR137B expressing and control Lamp1 expressing cells. There is a sharp expression dependence of mTORC1 translocation on RagC expression only when co-expressed with GPR137B. Error bars represent mean ± SD and n=3 independent experiments. (**e**) GPR137B co-expression with wildtype RagA/C in RagA/B−/− MEFs promotes RagA/C expression-dependent mTORC1 translocation in the absence of amino acids, and this effect is significantly lower in RagA/B−/− MEFs co-expressing GPR137B and dominant negative RagA/C (RagA T21L/RagC Q120L). RagA/B−/− MEFs transiently expressing either Lamp1 as control or GPR137B, along with WT or DN Rag A/C proteins, starved for 2hrs, fixed and stained for mTOR and Lamp2. In **c, d** and **e**, RagC expression is used as a readout of RagA/C dimer expression.

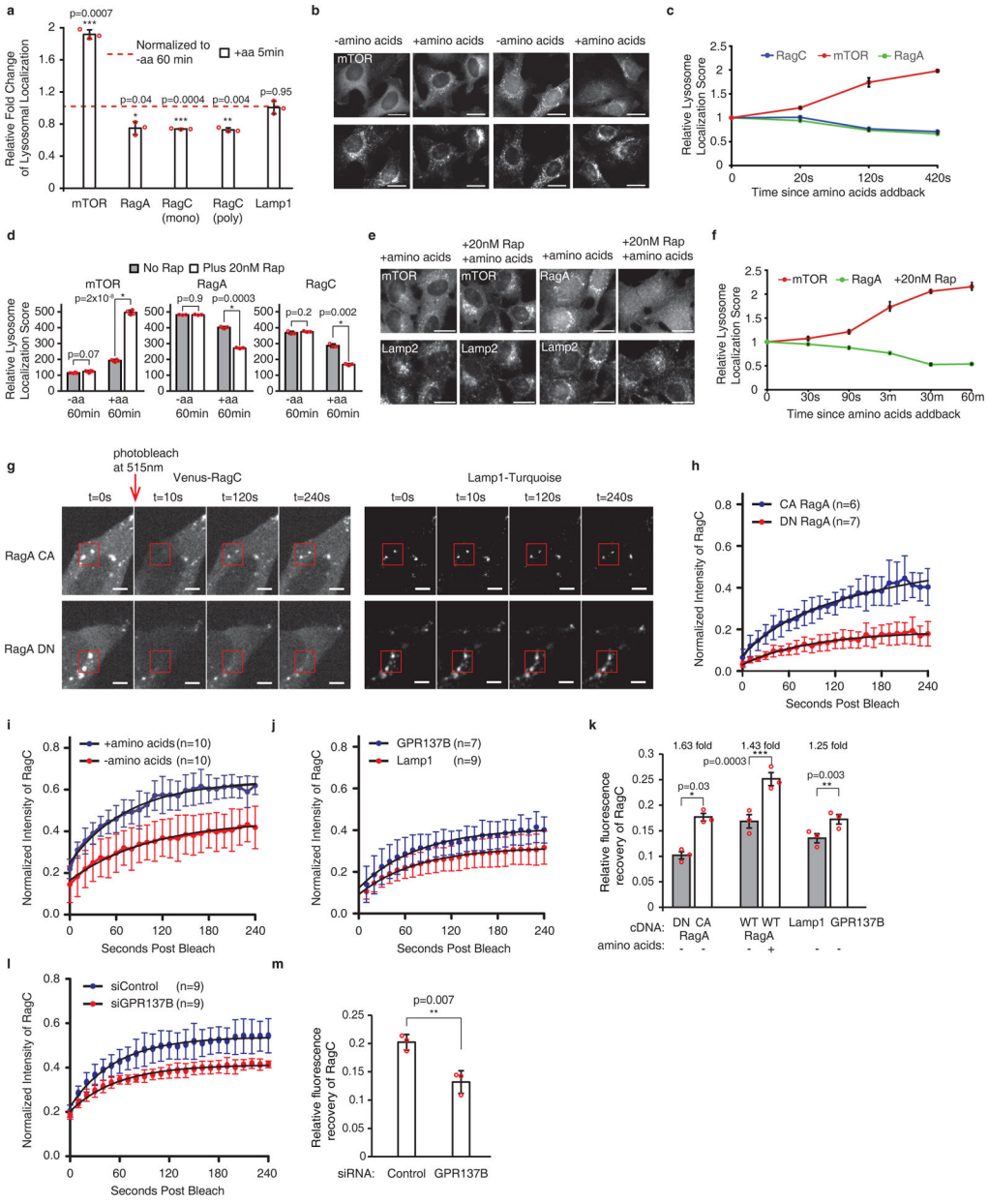

Figure 6: Evaluation of the role of GPR137B in regulating Rags by monitoring changes in the exchange rate of RagA/C from lysosomes

(**a**) Endogenous Rag A/C dissociates from lysosomes upon amino acid stimulation (HeLa cells). Co-localization analysis as in Fig. 2. Error bars, mean ± SD, 3 independent experiments (P values, two-tailed Student's t-test). (**b**) Representative images of mTOR and RagA staining as in **a**. Scale bar, 20 μm. (**c**) RagA and RagC dissociate from lysosomes with kinetics anti-correlated with mTOR translocation. Stained as in **a**. Mean ± SD, 3 independent experiments. (**d**) Rapamycin increases lysosomal retention of mTOR and accelerates dissociation of RagA and RagC. Stained as in **a** (mean ± SD, 3 independent experiments; P values, two-tailed Student's t-test). (**e**) Representative images of endogenous mTOR and RagA, stained as in **d**. Scale bar, 20 μm. (**f**) Endogenous RagA dissociates from

lysosomes with kinetics anti-correlated with mTOR translocation (with rapamycin), stained as in **a**. Mean ± SD, 3 independent experiments. (**g**) Photobleaching recovery measurements of RagC exchange. Lysosome-localized, constitutively active Rag increases the exchange rate of bleached Venus-RagC from lysosomes. RagA CA (HA GST RagA66L) (*top*) or RagA DN (HA GST RagA21L) (*bottom*) paired with wildtype Venus-RagC before (frame 1) and after photobleaching (frame 2–4). Red box denotes lysosome. 10s time-points, confocal microscope at 40x. Scale bar, 5 μm. (**h**) Averaged photobleaching recovery curves ± SD for RagA CA (n=6 cells) and RagA DN (n=7 cells). (**i**) Lysosomal Venus-RagC intensity recovers faster with than without amino acids. n=10 cells each. (**j**) Lysosomal Venus-RagC intensity recovers faster when co-expressed with GPR137B compared to Lamp1 as control. Lamp1, n=9 cells and GPR137B, n=7 cells. In (**h-j**), error bars, ± SD of the mean, intensities normalized to intensity before photobleaching. (**k**) Bar graph representation of data in **h-j**. n=3 independent experiments, error bars mean ± SD (P values, two-tailed Student's t-test). (**l, m**) Lysosomal Venus-RagC intensity recovers slower in cells treated with siGPR137B compared to siControl. Lamp1, n=9 cells and GPR137B, n=9 cells. (**m**) Bar graph representation of data in (**l**). n=3 independent experiments, error bars representing mean ± SD (P values, two-tailed Student's t-test).

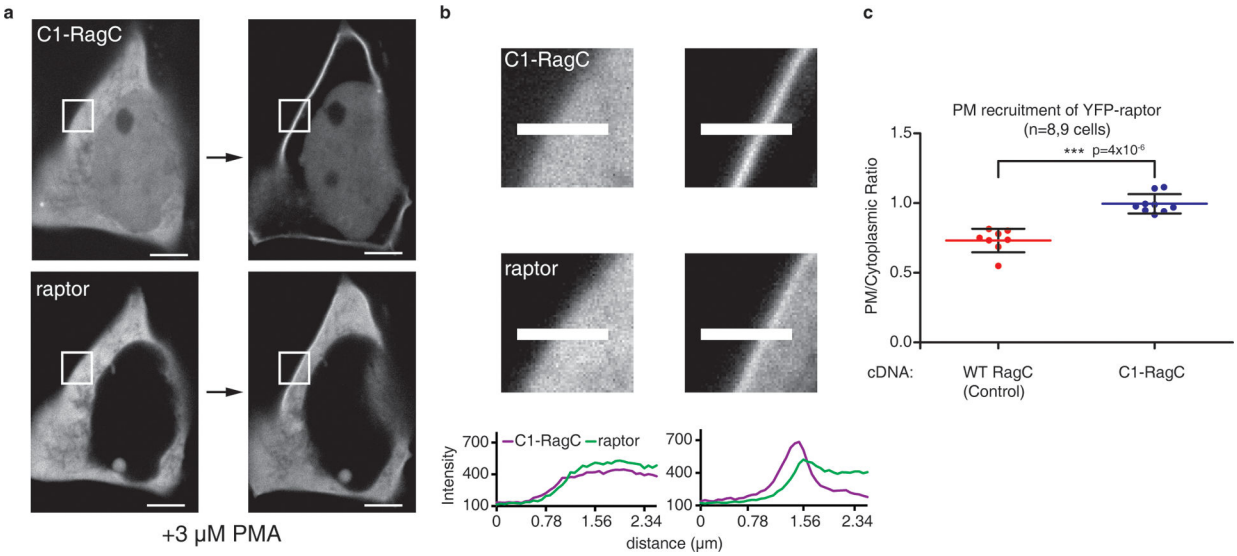

Figure 7: Active Rag and raptor can rapidly diffuse in the cytoplasm while being in a complex

(**a**) Raptor translocates to the plasma membrane along with C1-domain tagged RagC upon addition of phorbol myristate acetate (PMA). Images of HEK293Ts transiently transfected with YFP-raptor, C1-mRuby-RagC, and HA-CA RagA (RagAQ66L) before and after 3uM PMA. Scale bar, 5μm (**b**) Magnified images of raptor and C1-RagC translocation to the plasma membrane and line scan profiles measuring the intensities across the plasma membrane edge. White lines indicate positions of the line scan profiles (**c**) Quantification of plasma membrane to cytoplasmic intensity ratio of YFP-raptor in cells expressing either wildtype RagC or C1-RagC, along with YFP-raptor, HA-CA RagA and iRFP-CAAX. Only low YFP-raptor expressing cells are analyzed. n=3 independent experiments with error bars representing mean ± SD and P value is calculated from two-tailed Student's t-test.

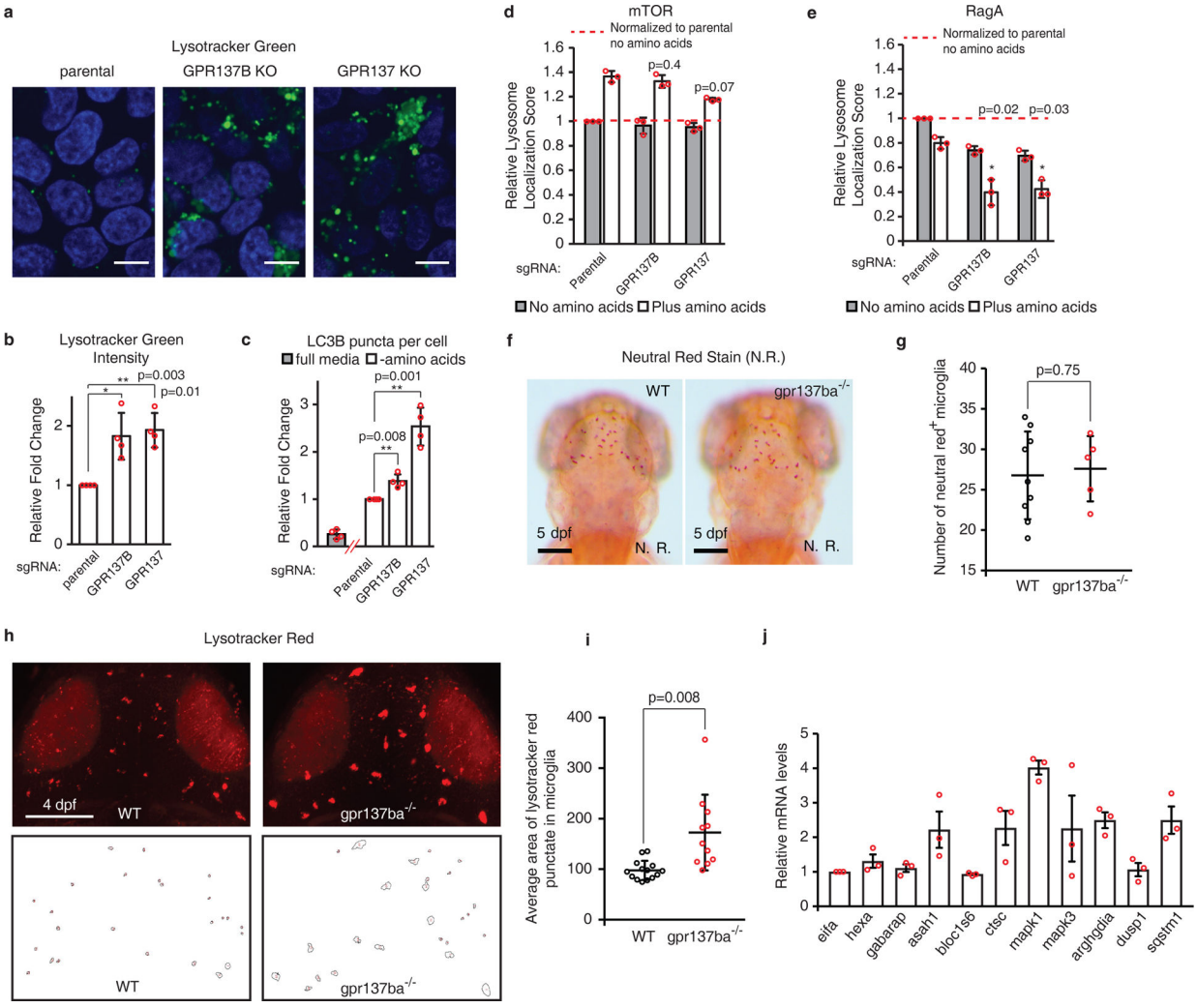

Figure 8: Knockout of human GPR137B and *gpr137ba* zebrafish mutants show defects similar to Rag pathway mutants

(**a, b**) Confocal images of HAP-1 parental, GPR137B KO and GPR137 KO cells stained with Hoechst and Lysotracker Green. Quantification in **b**. (**c**) HAP-1 GPR137 KO and GPR137B KO cells have increased number of autophagosomes and/or autolysosomes as measured by endogenous LC3B puncta in response to amino acid starvation. KO clones have statistically significant upregulation from parental. In **b** and **c**, mean ± SD, n=4 independent experiments, ratio paired t-test. (**d**) Amino acid-induced mTOR translocation is not statistically significantly different in HAP-1 GPR137B KO and GPR137 KO cells. (**e**) Lysosomal localization of RagA is reduced in HAP-1 GPR137B KO and GPR137 KO cells. Every KO has statistically significant downregulation from parental. n=3 independent experiments in **d**, **e.** Error bars representing mean ± SD (one-way ANOVA analysis followed by Tukey's test). (**f**) Wildtype and *gpr137ba*$^{-/-}$ zebrafish have comparable numbers of neutral red positive microglia. **(g)** Quantitative analysis of (**f**) using unpaired, parametric, two-tailed t-test with Welch's correction (p=0.75), wildtype n=9 animals, *gpr137ba*$^{-/-}$ n=5 animals. Center values indicate mean and error bars represent SEMs. (**h**) LysoTracker Red staining in wildtype (*left*), and *gpr137ba*$^{-/-}$ zebrafish larvae (*right*), show enlarged

lysosomal compartments in the microglia of *gpr137ba*$^{-/-}$ fish. Scale bar, 50 μm. LysoTracker Red positive compartments are segmented and analyzed for area in wildtype and *gpr137ba*$^{-/-}$ (*bottom*). **(i)** Quantification of area of LysoTracker Red punctae in zebrafish microglia shows that *gpr137ba*$^{-/-}$ larvae (n=11) have significantly (p=0.008) larger LysoTracker Red positive compartments relative to wildtype larvae (n=14). Data points represent the average area of the punctae in a single animal. Mean values and SEMs shown (unpaired, parametric, two-tailed t-test with Welch's correction). (**j**) Quantitative PCR analysis of Transcription Factor EB targets in pooled *gpr137ba*$^{-/-}$ zebrafish relative to a pool of heterozygous (*gpr137ba*$^{+/-}$) controls (n=15–16 animals in each pool); mutations in *gpr137* and *gpr137c* are randomly assorted in the pools (see text and Methods). Targets of TFEB significantly upregulated by comparing ΔCt values: *arghgdia* p=0.01, *mapk1* p=0.001, *sqstm* p=0.001, *ctsc* p=0.05. Mean values and SEMs shown (unpaired, parametric two-tailed t-test with Welch's correction).